Titel

Retrograde Control of Cytosolic Translation Targets Synthesis of Plastid Localized Proteins and Nuclear Responses for Efficient Light Acclimation.

Marten Moore[1,2], Aaron Smith[2], Corinna Wesemann[1], Sonja Schmidtpott[1], Melanie Wegener[1], Muhammad Ansar Farooq[1], Thorsten Seidel[1], Barry Pogson[2] and Karl-Josef Dietz[1§].

[1]Biochemistry and Physiology of Plants, Bielefeld University, 33501 Bielefeld, Germany.

[2]ARC Centre of Excellence in Plant Energy Biology, The Australian National University, Canberra, ACT 2601, Australia.

Keywords: High light, chloroplast, retrograde signalling, stress acclimation, transcriptome, translational control,

§ Address for correspondence

Karl-Josef Dietz§
Biochemistry and Physiology of Plants – W5-134
Bielefeld University
33501 Bielefeld
Germany
Tel. +49 521 1065589
Fax. +49 521 1066039
E-mail: karl-josef.dietz@uni-bielefeld.de

List of Abbreviation: ABA: abscisic acid; *A. thaliana*: *Arabidopsis thaliana*; AKIN10: protein kinase being part of the sucrose non-fermenting kinase complex; Asc: ascorbate; CaM: calmodulin; CML: calmodulin-like; DEG: differentially expressed gene; DHA: dehydroascorbate; GAPC: glyceraldehyde-3-phosphate dehydrogenase 2; GCN2: general control non-repressible 2; GO: gene-ontology; GSH: glutathione; GSSG: glutathione disulfide; H-light: Highlight (800 µmol photons m^{-2} s^{-1}); H_2O_2: hydrogen peroxide; HSE: heat shock element; HSF: heat shock factor; HSP: heat shock protein; IRES: independent ribosomal entry sites; JA: jasmonic acid; L-light: Lowlight (8 µmol photons m^{-2} s^{-1}); log_2: logarithmic fold change to base 2; MAPK: mitogen-activated protein kinase; mbSUS: mating-based Split-ubiquitin-System; *O. sativa*: *Oryza sativa*; OPDA: 12-oxo-phytodienoic acid; ORF: open reading frame; PEG: polyethylene glycol; PET: photosynthetic electron transport; RBP: RNA binding protein; PPLT: preferentially polysome-loaded transcript; PPUT: preferentially polysome-unloaded transcript; ROS: reactive oxygen species; SAP: stress associated protein; SnRK1: SNF1-related kinase 1; TE: translation efficiency; TF: transcription factor; TOR: target of rapamycin; TPT: triosophosphate/phosphate translocator; UTR: untranslated region; VTC2: GDP-L-galactose phosphorylase;

Abstract

Canonical retrograde signaling is the transmission of information from organelles to the nucleus. Discrepancies between protein accumulation and transcript abundance in response to oxidative stress were suggestive of protein translation responding to retrograde signaling. Here we uncover multiple components of a translation-dependent retrograde signaling pathway that impact translation efficiency and gene expression, including the kinases, MPK6 and the SnRK1 subunit, AKIN10. Global ribosome foot-printing demonstrated rapid differential loading of 939 of transcripts from polyribosomes within 10 min after transfer from Low to High-light. Translationally regulated transcripts shared motifs in their 5`-UTR that act as binding sites for RBPs such as GAPC. The Stress Associated Proteins 2 and 3 carry such motifs in their UTRs and interact with the calcium sensor Calmodulin-like 49, relocating to the nucleus to co-regulate a translation-dependent transcriptional response. Translation dependent retrograde signaling bifurcates into a direct translational circuit and a translation-reliant nuclear circuit synchronizing translation, nuclear and anterograde response pathways, which may serve as a just in time-provision of needed proteins to the plastids.

52 # Introduction

53 **Introduction**

54 Light impacts plant morphogenesis, development and metabolism. Gains in biomass and fitness
55 strongly correlates with light-dependent photosynthesis, with starch accumulating during the light
56 phase being essential for metabolism and growth during the dark phase. However, excess light
57 leads to an over-reduction of the photosynthetic electron transport (PET) chain and enhances
58 production of reactive oxygen species (ROS) (1). The natural light environment fluctuates
59 continually on the time scales of seconds, hours and days. To cope with rapid light fluctuations,
60 plants control their capacity to dissipate excess energy and minimize photo-oxidative damage (2).
61 ROS accumulating in excess light are detoxified by the water-water cycle in an ascorbate-
62 dependent or ascorbate-independent process utilizing ascorbate peroxidases and peroxiredoxins,
63 respectively (3, 4). On longer time scales, changes in light quantity alter photosystem stoichiometry
64 and increase the photosystem repair capacity.

65 Proteins of the photosynthetic machinery are encoded in the plastome and the nuclear genome
66 while all antioxidant enzymes are exclusively encoded in the nucleus, as is the majority of the
67 plastidial proteins. Transcription, stability and translation of chloroplast mRNA strongly depends
68 on nuclear genome-encoded sigma factors and RNA binding proteins (RBPs) (5). The
69 reorganization of photosystems and readjustment of the antioxidant systems, therefore, rely on a
70 coordinated production of nucleus- and chloroplast-encoded proteins (6). Coordination is realized
71 by transmitting information on the metabolic state of the chloroplast as retrograde signals to the
72 nucleus. Alterations in light quality and quantity result in fluctuations of metabolites and signal
73 export from the chloroplast with impact on accumulation and stability of mRNA.

74 Several signaling pathways are involved in developmental and operational retrograde control of
75 nuclear gene expression. They include signals from the plastoquinone and carotenoid pools,
76 tetrapyrrole biosynthesis, dihydroxyacetone phosphate (DHAP), reactive oxygen species (ROS),
77 ascorbate/dehydroascorbate (Asc/DHA) and glutathione/glutathione disulphide (GSH/GSSG),
78 hormones like 12-oxo-phytodienoic acid (OPDA) that also functions as precursor for jasmonic acid
79 (JA), and xanthoxin as precursor of abscisic acid (ABA), the SAL1/PAP pathway and sugars (3, 6-
80 16). Rapid regulation of transcription in response to excess light involves export of
81 triosephosphates, such as DHAP, via the triosephosphate/phosphate translocator (TPT2) and

82 Mitogen Activated Protein Kinase 6 (MPK6) and couples to the upregulation of a set of
83 Apetala2/Ethylene Response Factor (AP2/ERF) transcription factors (16). It is worth noting that
84 TPT2 co-controls the export of the DHAP retrograde signal (17). Transcriptome analyses (RNA-
85 seq, qPCR, sRNA-seq, and PARE) during repeated excess-light stress and recovery revealed
86 global, rapid and specific changes in transcript accumulation and rate of decay in response to
87 changing light regimes (18).

88 The retrograde signaling pathways identified to date target transcriptional control, while cytosolic
89 translation as a retrograde target of photosynthesizing chloroplasts is mostly unexplored,
90 particularly at rapid signaling time scales. While there are descriptive studies focusing on the
91 effects of translational control under the effects of the highly discussed gun mutants (19), very little
92 evidence of the mechanisms of cytosolic control of translation as a consequence of retrograde
93 signaling is available. This gap in knowledge needs to be closed since translational control has the
94 potential for more immediate spatial and temporal adjustment of the chloroplast proteome and may
95 better account for proteins whose abundance is regulated post-transcriptionally. Redox regulation
96 of the translational apparatus has been suggested as one such translational control mechanism (20).
97 Recently, a link between the light stress-associated increase in ROS leading and the rapid activation
98 of GCN2 kinase, thus inhibiting the translation initiation pathway of GCN2-eIF2α, has been
99 reported (21). This process also affected the translation of transcripts encoding mitochondrial ATP
100 synthesis and chloroplast thylakoid proteins.

101 Post-transcriptional regulation of mRNA stability and translation is known from circadian
102 rhythmicity and involves light entrainment (22). mRNAs encoding enzymes of central metabolism
103 associate with the ribosomes in dependence on light and input from the circadian clock. The impact
104 of circadian rhythmicity on the steady-state pool of polysome-recruited transcripts was lost if the
105 shift to darkness or re-illumination occurred out of phase (23). The energy sensor kinase AKIN10
106 entrains the circadian clock depending on light input (24). AKIN10 is part of the Sucrose Non-
107 Fermenting 1-Related Kinase 1 (SnRK1) complex and acts as a central regulator of transcription
108 and translation networks via the TOR complex (25-27).

109 We felt that there is a fundamental need to address the significance and mechanism of translational
110 regulation of light acclimation by retrograde signaling. Retrograde control of vicinal translation is

111 hypothesized as straightforward mechanism for chloroplasts to influence their protein complement
112 in a much faster way or even totally independent on nuclear gene expression.

113 To challenge this hypothesis, global polysome loading was used as readout of current protein
114 synthesis of Arabidopsis leaves following a 10 min exposure to H-light. Results revealed a rapid
115 reorganization of the translatome and identified a set of preferentially polysome-associated
116 mRNAs. Among the stress-associated proteins with Zn-binding domains, SAP2 and SAP3 attracted
117 our attention. The calmodulin-like protein CML49 was an interacting partner of SAP2 and SAP3.
118 Transcript profiling of *sap3* and *cml49* knockout lines following H-light exposure revealed
119 downstream target genes critically involved in light acclimation. Finally, the centrality of the
120 AKIN10 kinase in coordinating energy availability, metabolic activity and stress placed this kinase
121 in the focus of this work on retrograde control of translation. This study provides first conclusive
122 evidence for rapid retrograde effects on cytosolic translation.

123 **Results**

124 **Rapid initiation of retrograde translational signaling**

125 The rapid reorganization of the translatome was addressed in Arabidopsis whole rosettes following
126 a sudden change in photosynthetic irradiance. We used our established shift treatment of low (L-
127 light) (8 µmol photons m^{-2} s^{-1}) to H-light (800 µmol photons m^{-2} s^{-1}) for 0 or 10 min (L→H-transfer)
128 or by returning to L-light for 10 and 50 min (L→H→L) prior to harvest consistent with established
129 analyses (16, 28). To assess the effect of retrograde signaling on translation, mRNAs associated
130 with multiple ribosomes (polysomes) were isolated to identify actively translated mRNA, via
131 comparison with the global mRNA population (total RNA). To this end, ribosomes were arrested
132 on their correspondent mRNA and isolated through sucrose gradient centrifugation, subsequently
133 RNase I-digested and the resulting ribosome-protected fragments processed for polysome-
134 protected fragment sequencing (translatome) in parallel to total RNA sequencing (total
135 transcriptome) as described (29). The traditional ribosome stalling reagents for this protocol are
136 cycloheximide and chloramphenicol which mainly stall the 80S ribosome. Additionally, the 70S
137 ribosome inhibitor lincomycin was used during polysome extraction and following protocol steps.
138 This change in protocol allowed for the first time the simultaneous assessment of cytosolic
139 translation as well as translation in mitochondria and chloroplasts. The fraction of polysome-loaded
140 mRNA strongly declined after 10 min of L→H-transfer, but exceeded the control level after

141 transfer from L→H→L for 10 or 50 min (Figure 1 a, Suppl. Fig. 1 f-g.). The results indicate a rapid
142 unloading and reloading of polysomes in response to changing light conditions.

143 Translation efficiency (TE), defined as relative ribosome loading, was calculated by dividing the
144 abundance of a given transcript in the ribosome-associated fraction by its abundance in the total
145 RNA pool, normalized by library size. The TE is therefore a measure of the proportion of
146 transcripts for a given gene undergoing active translation at a given time. A set of 939 transcripts
147 (false discovery rate (FDR) adjusted p-value (padj) < 0.05) was differentially loaded after short-
148 term exposure to H-light (Figure 1 b, Suppl. Dataset 1). The group of TE-downregulated transcripts
149 (571) exceeded that of TE-upregulated (368) transcripts by a factor of 1.55 (Figure 1 b), further
150 supporting the finding of global downregulation of translation after L→H-transfer. The comparison
151 of transcripts with altered polysome association relative to total abundance unveiled more
152 regulation at the translational than transcriptional level. Sets of 289 and 442 transcripts with
153 increased or decreased abundance responded only translationally, whereas much smaller sets of
154 128 (up) and 51 (down) transcripts were exclusively transcriptionally regulated (Figure 1 c).

155 The key question is how excess light triggers a change in translational efficiency and was addressed
156 by scrutinizing known translation-regulating factors. MAP kinase-dependent phosphorylation of
157 the SnRK1 subunit AKIN10 leads to regulation of translation via TOR signaling and we have
158 previously shown that MPK6 phosphorylation depends on functional TPT, which exports DHAP
159 as retrograde signal (30). The dynamic unloading of ribosomes during L→H seen in the WT
160 genotype was absent in *akin10* and was dampened in *mpk6* background as could be visualized via
161 polysomal profiling and fractioning (Suppl. Fig. 1 f-g.). To assess the shift of polysome-associated
162 mRNAs not only quantitatively but also qualitatively, we selected 89 transcripts whose
163 translational efficiency increased. This set contained photosynthesis and stress response genes such
164 as *SAP2* and *SAP3*. In addition, we selected three genes from the 442 transcripts whose translational
165 efficiency decreased, namely *ERF105*, *HSP70* and *DREB2A*. All five transcripts showed increased
166 polysome-loading in response to 10 min H-light but either showed increased or decreased
167 translational efficiency due to changing total mRNA amount. Compared to WT, TE of 4 of the 5
168 transcripts was significantly altered in *akin10* background, with *SAP2* and *HSP70* also being
169 significantly altered in *mpk6* background (Suppl. Fig. 1 a-e. and Suppl. Table 1). Interestingly, the
170 increase of TE of *SAP2*, *SAP3* and *HSP20* was diminished in *akin10*, while the decrease of TE in
171 *ERF105*, *DREB2A* and *HSP70* was less accentuated.

172 **Evidence for a translational retrograde circuit enriched in photosynthesis proteins**

173 Clustering of the differentially accumulating transcripts in the polysomal versus total RNA
174 fractions allowed discrimination of subsets that revealed distinctive regulatory responses (Figure 1
175 d.). Cluster 1 includes transcripts that exclusively increase their polysome loading, while total
176 mRNA abundance was insignificantly changed (119 DEGs; preferentially polysome-loaded
177 transcripts; PPLT). Transcripts of cluster 2 are unloaded from polysomes (466 DEGs; preferentially
178 polysome-unloaded transcripts PPUT). Both clusters were significantly altered in polysomal fold-
179 change but not significantly altered in total RNA fold-change. Clusters 3 and 4 comprise transcripts
180 that upon transfer to H-light simultaneously changed in the polysomal and total RNA fraction, 62
181 up and 123 down regulated DEGs (cluster 3 and 4, respectively; Figure 1 d; Poly and Total). Others
182 were not assigned to clusters, e.g., 33 DEGs that were changed in total mRNA but not in the
183 polysomal fraction and termed as buffered transcripts.

184 The polysome-loaded cluster (PPLT, Cluster 1) was five-fold enriched in transcripts coding for
185 chloroplast-localised proteins according to SUBA4 (31). Among those, GO terms for
186 photosynthesis are highly overrepresented (8.7 % in comparison to 0.5 % of genome
187 representation), in particular for photosystem II light harvesting (1.9 %). Those include minor
188 (AT3G47470) and major light harvesting proteins (AT4G10340), subunits of photosystem I
189 (AT2G46820), one of the two nuclear encoded cytochrome b6f subunits (AT2G26500) and
190 NADPH oxidoreductase subunits participating in electron transport (AT1G06690) as well as *small*
191 *subunits of RuBisCO* (AT5G38410) (see Suppl. Dataset 1, PPLT). Apart from photosynthetic
192 proteins, this set included proteins participating in assembly, damage and repair, e.g., chloroplast-
193 localised *HSC70-1* (AT5G02500), which is involved in protein import; chloroplast vesiculation
194 factors (AT4G32150) taking part in partitioning damaged proteins for proteolysis; and
195 *PYG7/YCF37* (AT2G23670) which is required for PSI assembly/repair. The transcripts coding for
196 cytosolic proteins were enriched in GO terms for translation (15 % in comparison to 4.9 % of
197 genome representation), e.g., proteins of *ribosomal large subunit* (AT3G08520).

198 Cluster 2 comprising solely translationally downregulated DEGs (PPUT) (Figure 1 d) was enriched
199 in multiple GO terms, e.g., response to auxin 5.7 %, chlorophyll biosynthetic process 2.0 % and
200 response to far red light 2.6 %, but a prevailing response was undetectable. The transcripts
201 upregulated both in the polysomal and total fraction in cluster 3 (Figure 1 d, poly and total) were
202 enriched in abiotic stress GO terms: heat stress (48.1 % in comparison to 0.5 % of genome

203 representation); response to hydrogen peroxide (20.3 %); and light stimulus (20.3 %; Suppl.
204 Dataset 1). This cluster included small (*HSP20-likes*) and large heat shock proteins (*HSP70*,
205 *HSP101*), their organizing factors (*HOP*) as well as their key regulatory transcription factors
206 *HSFA2* (AT2G26150), *HSF2BA* (AT5G62020), *HSFB2B* (AT4G11660) and *DREB2A*
207 (AT5G05410).

208 **Plastid translation regulated in response to rapid light shift**

209 While cytosolic translation was increased for photosynthetic transcripts, plastid translation
210 revealed as translationally upregulated transcript only chloroplast-encoded PSBA coding for the
211 PSII subunit D1. No mitochondrial transcripts were detected as translationally upregulated.
212 Interestingly, 36 and 16 DEGs of chloroplast and mitochondria representing 42.9 % and 34 % of
213 detected plastidial transcripts, respectively, were decreased in translation (PPUT cluster). The
214 translational downregulated transcripts were highly enriched in GO terms for translational
215 processes (30 % in comparison to 0.6 % of genome representation) and ribosome assembly (11 %
216 compared to 0.09 %) and photosynthetic light reaction (11 % to 0.11 %) represented by *YCF3* and
217 *4* (ATCG00360, ATCG00520), PSII *CP47* reaction center protein (ATCG00680) and *NDH H*
218 (ATCG01110). No enrichment in particular GO terms could be detected in the mitochondrial
219 DEGs, but 6 of the 16 DEGs encoded for NADH dehydrogenases.

220 **Translationally regulated transcripts are enriched in regulatory short mRNA motifs**

221 Efficient reorganisation of translation requires unloading of ribosomes and reloading with
222 preferably required transcripts. Translation initiation factors instigate translation in concert with
223 mRNA regulatory sequences and/or structures. Often the 5'-UTR and 3'-UTR possess features that
224 influence the initiation rate, like independent ribosomal entry sites (IRES). Therefore, the 5'- and
225 3'-UTRs of the clusters PPLT, PPUT and poly and total transcripts were screened for conserved
226 motifs enriched against all TAIR annotated 5'-UTRs or 3'-UTRs using the MEME-suite (32). The
227 search identified 40 motifs in the UTRs from which three were selected based on their
228 overrepresentation in the PPLT (Cluster 1) and poly and total cluster (Cluster 3) (M1:
229 TCTCCGGAGAA, M2: TTAGGGTT and M3: TCGCCG). M3 is a subsequence of M1 (Figure 2).
230 M2 has previously been identified as stress-responsive 5'-UTR element that confers preferential
231 translation in vitro (33). M1 and M2 were present 40- and 34-times in the 5'- and 3'-UTRs of the
232 transcripts preferentially associating with ribosomes in H-light, accounting for 31% and 26%,

233 respectively. M2 is present in transcripts that are exclusively translationally regulated and not
234 transcriptionally, whereas M1 and M3 are also present in transcriptionally regulated transcripts
235 (Suppl. Fig. 2 c). Transcripts carrying M1 and M2 had a median relative translation rate of 2.09
236 and 1.97, respectively, and relative to the median translation rate of 2.96 of all PPLT transcripts.
237 Transcripts carrying M3 had a higher relative translation rate of 3.57 (Suppl. Fig. 2 d). Heat-
238 responsive transcripts like *HSFB2B* and *HSP20*-like proteins, as well as other stress-dependent
239 transcripts, were overrepresented among the motif-carrying transcripts. Interestingly the UTRs of
240 the *Stress Associated Protein 3* (*SAP3*) carries all three motifs and *SAP2* UTR carries M2 (Suppl.
241 Fig. 2 a, b). SAPs belong to the family of zinc finger proteins that contain A20/AN1 zinc-binding
242 domains. They are structurally and functionally conserved among diverse plant species (34). *SAP*
243 transcript amounts increase in response to multiple stresses, and overexpression of specific SAPs
244 in planta enhances biotic or abiotic stress tolerance or photosynthetic capacity (35, 36). A
245 significant increase in ribosome loading after 10 min of L→H could be verified via qPCR for the
246 transcripts of *HSP70*, *ERF105*, *DREB2A*, *SAP3* and *SAP2* with no significant increase in total
247 mRNA for *SAP2* (Suppl. Fig. 1). SAP2 was highly enriched in the polysomal fraction, hence
248 preferentially recruited to the polysomes. To assess importance of the motifs on an evolutionary
249 scale we queried the rice genome and identified *OsSAP8* and *OsSAP9* as putative rice homologues
250 of *SAP2* and *SAP3* and detected variations of all three motifs in their respective 5'-UTRs (Suppl.
251 Fig. 4). Additionally, we observed the preferential association of transcripts for *OsSAP8* and
252 *OsSAP9* with polysomes upon L→H transfer in rice (Suppl. Fig. 5).

253 **Retrograde translational signaling is mediated by conserved motifs in the 5' UTR that serve**
254 **as potential target for RNA binding proteins**

255 Position analysis in the respective 5'-UTR of motif-carrying transcripts revealed a preferred
256 position at the 3'-end in longer UTRs, while short UTRs showed no positional preference (Suppl.
257 Fig. 2 b). Calculating the secondary structure via RNA Shapes Studio revealed that the motifs do
258 not overlap with in any conserved secondary structure (Suppl. Fig. 2 b).

259 The hypothesized role in translational regulation of the three motifs was tested in a cell-based
260 luciferase reporter assay. Cassettes carrying the M1, M2 or M3 motifs in triplicate repeats were
261 inserted into the ubiquitin 5'-UTR in front of firefly luciferase reporter and the verified constructs
262 transiently co-transfected together with pGL4::Renilla Luciferase as reference reporter into A.
263 thaliana mesophyll protoplasts (Figure 2 b). The protoplasts were treated analogously to the whole

264 plant experiments with L→H-transfer for 10 min. The normalized luciferase activity from lysed
265 protoplasts transformed with the ubiquitin 5'-UTR without motifs increased 2.5-fold after L→H-
266 treatment. All motifs conveyed a higher signal than the ubiquitin control with M1-construct causing
267 the highest increase of 5-fold, 1.75-fold for M3 and insignificant for M2 (1.52-fold) (Figure 2 c).

268 The potential mRNP-binding properties of the motifs were tested via RNA-EMSA. Biotinylated
269 M3-RNA was incubated with leaf protein extracts that were either prepared from L-light-
270 acclimated plants or plants exposed to L→H transfer for 10 min (Suppl. Fig. 3 a). Addition of
271 protein extracts from L-light exposed leaves resulted in a pronounced shift of signals in comparison
272 to the biotinylated M3-RNA control. Addition of unlabeled competitor M3-RNA strongly
273 suppressed the shift. Supplementation with extract from 10 min L→H-treated plants resulted in a
274 signal intensification that again was out-competed by competitor M3-RNA. This result suggests
275 mRBP binding capability of M3 with differences in protein signature in polysomal fractions
276 between L-light plants and 10 min L→H-plants. Proteins interacting with M1 and M2 were
277 detected via affinity pulldown purification and subsequent SDS-PAGE revealed enrichment of
278 specific bands of which two were identified as GAPC2 and ATP synthase subunit alpha binding to
279 M2 and M1, respectively (Suppl. Fig 3 b-d).

280 Targeted RNA-EMSA with recombinant AtGAPC1 as RBP candidate showed a concentration
281 dependent band shift of free consensus M1- and M2-RNA (Suppl. Fig 3 e). To scrutinize these first
282 indications, interaction with the native M1 motif of the SAP3 5'UTR was used for affinity pull
283 down of potential RBPs with total protein extracts from L-light- or L→H-light-treated plants.
284 Immunodetection of AtGAPDH isoforms C1 and C2 revealed a strong signal in the elution fraction
285 derived from L-light leaf extract, whereas the signal in the H-light fraction was comparatively
286 weak. For reference, the GapC1/C2 content showed no difference in the input extract from L-light-
287 compared to H-light-plants. The same probe (SAP3 M1) was also used for RNA-EMSA with
288 recombinant AtGAPC1, C2 or GAPDH isolated from rabbit muscle to validate the interaction
289 between the motif-carrying RNA and GAPDH in vitro. Like above, adding increasing amounts of
290 protein led to a band shift of the free RNA. This shift was suppressed by adding unlabeled
291 competitor RNA.

292 **Synchronization of translational signaling and nuclear transcription: CML49 interacts with**
293 **SAPs to integrate translational, redox and calcium signaling**

294 Rapid translational regulation of stress-responsive transcription factors and co-factors like MBF1c,
295 HSF2A and DREB2A suggests integration of cytosolic translation in synchronizing plastid demand
296 and nuclear transcription. These factors are known to be involved in transcriptional regulation of
297 major stress response genes like HSPs and APX2 (37, 38). Other targets of translational control
298 were the transcripts of *SAP2* and *SAP3*. Our previous studies revealed redox-dependent
299 conformational changes of SAP12, another member of the SAP gene family (39). Analyzing SAP2
300 and SAP3 for disulfide bonds by DiANNA (40) revealed a predicted disulfide bond in the AN1
301 domains of SAP2 and SAP3 at Cys117 and Cys135. SAP2 compared to SAP3 has one additional
302 cysteine at position Cys8 which is predicted to form a disulfide bond with Cys22. Thus, SAP2 and
303 SAP3 might also function as redox sensory system in the translationally initiated retrograde
304 signaling network. The preferential association of SAP2 and SAP3 mRNA with polysomes after
305 L→H-transfer led us to search for interacting partners of these proteins. A yeast-two-hybrid screen
306 with SAP2 fused to the GAL4-DNA-binding domain as bait recovered six clones from the prey
307 consisting of Arabidopsis cDNA fused to the GAL4 activating domain, five of which coded for
308 Calmodulin-like 49 (CML49). The interaction between CML49 and SAP2 and SAP3 was
309 confirmed using the mating-based-Split-Ubiquitin (mbSUS) yeast-two-hybrid system (Figure 3 a)
310 and by fluorescence resonance energy transfer (FRET) (Figure 3 b, c). SAP2 and CML49 and SAP3
311 and CML49 co-localized in the nucleus (Figure 3 b) and showed a high FRET efficiency (> 5-fold
312 of negative control) proving their interaction in vivo (Figure 3 c). This interaction was also
313 confirmed for the SAP2/3 and CML49 homologues from rice (Suppl. Fig 6), thus seems to be a
314 conserved mechanism across multiple species.

315 The preferential association of *SAP2* and *SAP3* with polysomes after L→H-transfer and the
316 interaction of SAP2 and SAP3 with CML49 led us to hypothesize that CML49 and SAP2/SAP3
317 function as regulatory module in this specific environmental context. In addition, the similar
318 response of SAP2 and SAP3 in the L→H-response might indicate some functional redundancy.
319 With these two data-guided hypotheses in mind, we hypothesized that the CML49 knockout should
320 have stronger effects on downstream events during H-light acclimation than deletion of SAP3. To
321 investigate the importance of SAP3 and CML49 in H-light acclimation, we determined the
322 transcriptomes of *cml49*, *sap3* and WT in L-light and after 60 min L→H-transfer and calculated

323 the fold change as ratio of L→H/L (Suppl. Data Set 1). A set of 32 transcripts was more than 3-
324 fold increased or decreased in *sap3* relative to WT, while the corresponding set comprised 214
325 transcripts in *cml49*.

326 The data set was examined for transcripts that exhibited stronger downregulation in *cml49* than in
327 *sap3* upon L→H-transfer. This filter revealed 49 transcripts with the expected response pattern
328 (Figure 4 a). The predominant gene ontology groups belonged to the categories 'response to
329 temperature' and 'response to light stimulus', each of which represented 22 % of the genes,
330 followed by 'response to hydrogen peroxide' with 11 % and 'circadian rhythmicity' with 6 %. Heat
331 shock proteins and one heat shock factor (*HSFA2*) belonged to the group of heat responsive
332 elements, the *sigma factor 5* and *PSEUDO-RESPONSE REGULATOR 9* (*PRR9*) to the light
333 responsive elements *PURPLE ACID PHOSPHATASE 17* (*PAP17*) and the *GDP-L-galactose*
334 *phosphorylase VTC2* to the group of 'response to hydrogen peroxide'. *CIRCADIAN CLOCK*
335 *ASSOCIATED 1* (*CCA1*) and *PRR9* represent two genes associated with the circadian clock. The
336 occurrence of transporters for phosphate, sugar and sulphate (*PS3*, *AtSweet 13*, *GPT2*, *APR3*) in
337 this list indicates a function of CML49 and SAP3 in regulating metabolite and nutrient distribution.
338 Interestingly, the *translation elongation factor 1B* (*eEF1B*) was also found in this list possibly
339 pointing to SAP3/CML49-dependent amplification effects in the H-light dependent control of
340 translation.

341 The next experiments aimed to validate the deregulation of some of the identified transcripts and
342 to resolve the kinetics of their H-light induction (Figure 4 b-f). To this end, *sap3*, *cml49* and WT
343 plants were shifted from L-light to H-light for 10, 30 and 60 min. Plants left in L-light conditions
344 were used as control. Five targets were selected from the list of co-regulated transcripts for more
345 detailed analysis: *VTC2* showed a two-fold (log2) upregulation at t=10 in WT, followed by a
346 decrease to L-light levels at 30 and 60 min of L→H shift. In a converse manner, the response of
347 *sap3* and *cml49* displayed a steady decrease of transcript down to four-fold below the L-light level
348 (Figure 4 b-f). *HSP20*-like rapidly increased in WT upon L→H-transfer reaching its maximum of
349 six-fold (log2) induction at t=30 min and stayed constant until t=60 min. The mutants showed a
350 lower upregulation than WT with significantly reduced responses at t=10 and 30 min in *sap3* and
351 at 60 min in both mutants (Figure 4 b-f). The same trend appeared in WT for *PS3*, *SIG5* and *eEF1B*
352 with a two-fold upregulation after 10 until 60 min of L→H shift. The mutants showed a strong and
353 consistent deregulation compared to WT (Figure 4 b-f).

354 **Common cis-elements in promotor region of co-regulated genes**

355 The 49 co-regulated target genes were screened for common cis-elements in the promotor region
356 in order to find commonalities such as involved transcription factors (TFs) needed for expression
357 of the co-regulated gene set. A total of 9459 common cis-elements were identified in the 1000-bp
358 upstream region of the 49 genes (Suppl. Table 2). Most abundant common cis-elements were the
359 WBOX (2112), targeting sequences for the WRKY-TFs, followed by sulfur response (SURE) with
360 1536 and MYB and MYB-related with 1368 cis-element sequences. Stress related cis-elements like
361 the sequences overrepresented in light-induced promotors (SORLIPs) and early responsive to
362 dehydration (ABRE) were also highly abundant with 1278 and 1148, respectively. bZIP cis-
363 elements (C-box, 232), phosphate starvation (PHR1, 224) and salicylic acid inducible (LS7, 173)
364 were less abundant.

365 **Is there a translational retrograde – anterograde circuit?**

366 After 10 min L→H all plastidial translation is repressed with the sole exception of *PSBA*. This
367 correlated with increased ROS within chloroplasts and subsequent inhibition of plastidial
368 translation (16, 41). De-repression of plastidial transcription and translation during stress is
369 mitigated via sigma factors like SIG5 which contributes towards transcription of the psbD operon
370 (PSII D2) (42). Translational regulation of stress responsive transcription factors like HSF2A,
371 DREB2A, and the SAP2/3 interaction with CML49 leads to translation-dependent nucleus
372 synchronization after 10 min L→H. Plastid-targeted proteins like SIG5 and GPT2 and VTC2 were
373 transcriptionally upregulated in CML49- and SAP3-dependent manner but not preferentially
374 translated after 10 min L→H (Figure 4 b-e, Suppl. Dataset 1). Nonetheless, we hypothesize that
375 the SAP-CML49 co-regulated expression of SIG5 contributes to de-repression of chloroplast
376 genes, especially since PSII D2 transcription is 1.4-fold increased after 60 min of L→H.

377 ## Discussion

378 Regulation of actively translated transcripts described herein adds an entirely new mechanism to
379 retrograde communication in the cell. We identified components of the novel pathway of
380 translation-dependent retrograde signaling (TraDeRS) that bifurcates into direct translation of
381 chloroplast-targeted proteins. This process is completely uncoupled from nuclear transcription
382 (Figure 5 I.). In addition, retrograde control of cytosolic translation affects synthesis of a suite of
383 factors that in turn promote nuclear transcription. Both mechanisms enable the acclimation process

384 and are part of an anterograde response (Figure 5 II.). Collectively, the suite of chloroplast-targeted
385 and chloroplast-encoded proteins controlled by translation-dependent retrograde signaling includes
386 those involved in protein import and folding, chloroplast transcription, photosynthesis and
387 photoprotection.

388 **Evidence for translation-dependent retrograde signaling (TraDeRS)**

389 Translation-dependent regulation repressed global translation, while increasing translation of
390 stress-specific proteins within minutes of L→H-transfer (Figure 1 a, b). Our work demonstrates
391 that this process is rapidly and reversibly controlled under excess light (Figure 1 a). Most other
392 immediate short-term responses to excess light are chloroplast-located like non photochemical
393 quenching (43), malate valve stimulation (44) or activation of antioxidant metabolism (45). In
394 contrast to the chloroplast-localized processes, TraDeRS takes place in the cytosol and potentially
395 integrates multiple cues. Previously, we demonstrated that rapid transcriptional responses in the
396 nucleus affect a network of transcription factors within 20 s after the L→H-transfer (16, 46). This
397 included a H_2O_2 burst peaking at 30 min after the L→H (16). The decreased polysome association
398 of mRNA displayed a reciprocal behavior with the H_2O_2 burst after the L→H shift (16). The
399 maximal H_2O_2 accumulation after 30 min is followed by a return to basal levels after 60 min (16).
400 Parallel to the decreasing H_2O_2-content, general ribosome association of mRNA recovered after
401 one hour of H-light (Figure 1 a) (33).

402 **MPK6 and AKIN10 take part of translation-dependent retrograde signaling.**

403 Ribosome unloading and preferential loading of transcripts are decisive regulatory steps in
404 translational control and are mediated by translation initiation, elongation and termination factors
405 (47). The question is how does excess light in the chloroplast modulate translation? Protein
406 phosphorylation, thiol redox-related changes and acetylation are reported posttranslational
407 modifications (PTM) of involved translation factors and regulate translation initiation, elongation
408 and termination (16-19). Formation of the translational pre-initiation complex (PIC) is inhibited by
409 the General Control Non Derepressable-2 Kinase (GCN2) (48), and its activation has been shown
410 in to be linked to MAPK signalling pathways (49). Consequently, we investigated the involvement
411 of MAP kinases and showed that mutants lacking MPK6 exhibit an altered polysomal profile. The
412 mutant failed to realize the preferential ribosome loading of two of the markers of increased
413 translation, *SAP2* and *SAP3*, upon L→H-transfer (Suppl. Fig. 1).

414 The second rate-limiting mechanism of translation initiation is via the eIF4F complex formation
415 and subsequent mRNA binding regulated via 4EBPs. In mammals 4EBPs are activated by the
416 mammalian Target Of Rapamycin (mTOR) Kinase (50) mediating phosphorylation of the
417 eukaryotic Initiation Factor 4E (eIF4E), disabling interaction with initiation factor eIF4G, and thus
418 limiting eIF4F formation (51). Phosphorylation of the translation initiation factors eIF4E and
419 eIFiso4E via SnRK1, an interactor of TOR, inhibited translation in a plant system (52). Herein we
420 show that the lack of AKIN10, a subunit of the SnRK1, altered the polysomal profile compared to
421 WT under control and stress conditions and interfered with the preferential loading of the marker,
422 *SAP2*, onto ribosomes as well. A future question is what activates this pathway? ROS/Redox
423 regulation are candidates, as are GCN and TOR-signaling via AKIN10 and MPK6 (Suppl Fig. 1,
424 Suppl. Table 1) and DHAP. Of interest in this regard, we have previously reported that export of
425 DHAP from the chloroplast via the triosephosphate/phosphate translocator was required for rapid
426 phosphorylation of MAP Kinase 6 (MPK6) after 10 min L→H-transfer. In summary, the results
427 show that both MPK6 and AKIN10 are required for translation-dependent retrograde signaling,
428 most likely via a phosphorylation-dependent pathway.

429 **Proteins affected by bifurcating translation-dependent signaling pathways**

430 The set of preferentially loaded transcripts could be grouped into purely translationally regulated
431 and both, translation- and transcription-regulated transcripts, with each group representing distinct
432 regulatory bifurcation of acclimation responses. Transcripts related to photosynthesis, heat stress
433 and H_2O_2 dominated the set of preferentially polysome-loaded and motif-carrying transcripts.
434 Photosynthesis and chloroplast repair-related transcripts were highly enriched among the purely
435 translationally regulated transcripts (Suppl. Dataset 1, PPLT). The 119 transcripts in the
436 translation-alone regulatory cluster are 5-fold enriched in chloroplast-localized proteins according
437 to SUBA4 (31). This set includes proteins critical for assembly, function and maintenance of the
438 chloroplast. Minor and major light harvesting proteins like LHB1B1 (AT2G34430), LHCB3
439 (AT5G54270) and LHCB5 (AT4G10340), LHCA4 as a subunit of photosystem I (AT3G47470),
440 cytochrome b_6f (AT2G26500) and NADP oxidoreductase (AT1G06690) as well as one small
441 subunit of RuBisCO (AT5G38420). Additionally, PSI assembly factor PYG7/YCF37
442 (AT2G23670) and import chaperones like HSC70-1 (AT5G02500) and chloroplast vesiculation
443 factors (AT2G25625). Our results strongly suggest the existence of a transcription-independent

444 regulation of photosynthesis repair mechanism that is under rapid translation-dependent control
445 and forms a direct retrograde circuit (Figure 5, I. Direct Translational Circuit).

446 Complementary to photosystem repair, translational control of nuclear transcription factors (HSFs,
447 DREBs) synchronizes the gene expression with the cellular demand for subsequent stress
448 acclimation. The identified HSF2A, DREB2A and MBF1c play major roles in transcriptional
449 control of the H-light acclimation processes (53, 54). Interestingly, transcripts for these translation
450 factors are already present during LL-conditions but not preferentially translated (Suppl.DataSet
451 1). Preferential translation after stress perception might serve as first activator of these transcription
452 factors that are known to be up-regulated by oxidative stresses in general, and high light stress, in
453 particular.

454 **Regulatory elements controlling polysomal loading**

455 The regulation of specific mRNA translation efficiencies by targeting of different protein classes
456 for increased and decreased translation must be inherently based on their individual sequence or
457 structural properties. To identify conserved common sequences that might serve as such regulatory
458 property, we conducted *de novo* motif search for conserved sequences in the set of translationally
459 regulated transcripts via the MEME-tool suite to identify 42 motifs. In this study we could *in vivo*
460 demonstrate the impact of the three identified motifs during high light stress on translation and
461 provide evidence suggesting that they serve as mRNP binding sites including their interacting RBP
462 (Figure 2, Suppl. Fig. 3). RNA-EMSA shifts with leaf extracts from L- and L→H-light leaves
463 indicate that M3 acts as an mRNP binding site (Suppl. Fig. 3). Conditional mRNP-binding to motifs
464 1-3 stimulated polysomal loading and could be shown for motifs M1>>M3>M2 in a protoplast
465 transfection assay, the latter for M2 not being significantly different to the control (Figure 2). The
466 motif M2 (TAGGGTTT) has previously been identified in the 5'-UTRs of a set of preferentially
467 polysome-associated transcripts in young seedlings treated with light for 30 min, making it a
468 promising target for subsequent analysis. Translation of reporters from transcripts carrying the
469 motifs *in vitro* occurred at higher rates than from constructs lacking the sequence (33). The motif
470 was also overrepresented in preferentially polysome-associated transcripts under hypoxic stress
471 (55), suggesting a role for motif 2 under various stresses, but its mode of action is so far not
472 reported.

473 The nature of the RBPs that recognized the motifs M1 and M2 was investigated by RNA-based
474 affinity pull downs and protein identification via MS provided first candidate RBPs the ATP
475 synthase subunit alpha and GAPC2, respectively. GAPDH functions as non-canonical RBP in
476 animal systems (56, 57) and this role was only recently discussed in plants as well (58). We
477 validated the GAPDH-motif interaction using the native M1 of SAP3 5'-UTR via ex vivo affinity
478 pull down and subsequent immunodetection and in vitro by RNA-EMSA. These results point to
479 light-dependent protein-RNA interaction that possibly could mediate changes in TE upon L→H
480 shift. As protein amounts of GAPDH (C1/C2) were unaltered in L-light- or L→H-light-treated
481 plants conditional binding to RNA could be mediated by PTM or the availability of co-factors or
482 substrates. This would link translational control by RBPs to the cellular metabolic state enabling
483 the cell to rapidly adjust protein synthesis according to metabolic requirements. This hypothesis
484 needs further validation in detailed analysis.

485 ***SAP2* and *SAP3* contain motifs 1 and 2 and their proteins interact with CML49**

486 Motifs 1 and 2 are both present in the UTRs of *SAP2* and *SAP3* from Arabidopsis and also in their
487 homologues in the monocot rice. The transcripts in rice showed the same polysomal association
488 during L→H as in Arabidopsis. Interestingly, re-analyzing a dataset of Arabidopsis seedlings re-
489 illuminated after darkness for 10 min (23) for translationally regulated transcripts in the same
490 manner as performed for this study, revealed *SAP2* as one of only 5 transcripts overlapping with
491 the purely translationally regulated subgroup, PPLT (Suppl. Dataset 1).

492 The Stress Associated Proteins (SAPs) belong to a zinc-finger multigene family with a high level
493 of structural conservation and functional similarity among several plant species (34, 35). Despite
494 little knowledge on molecular function two regulatory roles have been attributed to SAPs, namely
495 ubiquitin ligase activity and redox sensor activity regulating gene expression under abiotic stress
496 (35, 39, 59, 60). Previous work demonstrated that AtSAP12 undergoes reversible redox-dependent
497 conformational changes induced by cellular redox changes during stress (39). This underlines the
498 possible role of SAPs as redox sensors during H-light acclimation. Furthermore, SAP5 interacts
499 with MBF1c during heat stress regulating heat acclimation responses via interaction with HSFs
500 and DREB transcription factors, ultimately influencing transcription (61). Given the structural
501 similarity between SAP2/3 and SAP5, the interaction of SAPs with MBF1c might co-regulate
502 specificity and interaction between HSFs, DREBs and MBF1c to synchronize transcriptional

503 demand, but remains subject to further study. Thus, retrograde signaling increases the abundance
504 of the protein and in parallel promotes its re-location to promoted transcript accumulation.

505 SAP2 and SAP3 interact with the Calmodulin-like-protein-49 (CML49). Based on the highly
506 conserved AN1 domain present in all members of the SAP protein family, an interaction of all
507 SAPs with CML49 is possible. Several CMLs display an electrophoretic mobility shift in the
508 presence of Ca^{2+}, indicating that they act as Ca^{2+} sensors (62, 63). Most CMLs lack known
509 functional domain impeding the prediction of biochemical functions. Nonetheless, CMLs are
510 important in signaling processes and are activated under stress conditions like heat, cold, drought
511 and heavy metals (64, 65). The Ca^{2+}-dependent binding of CaM7 to a Z-/G-box is involved in
512 regulating expression of light-responsive genes (66). H_2O_2 triggers an increase in cytosolic Ca^{2+}
513 by activating Ca^{2+} channels (67). Ca^{2+}¬-liganded CaM activates MPK8 which suppresses ROS
514 accumulation via transcriptional control of RbohD (68). *CML49* occurs in almost all tissues and
515 was not induced after 1 h of L→H-shift indicating that CML49 functions as constitutive signal
516 transmitter. Interestingly, the rice homologues of SAP2 and SAP3 also interact with CML49
517 homologues indicating a conserved regulatory mechanism potentially integrating ROS cues with
518 Ca^{2+} signaling (Suppl. Fig. 6) across multiple plant species.

519 **SAP3 and CML49 co-regulate transcript accumulation**

520 Both *sap3* and *cml49* knockouts display smaller sets of H-light-induced transcripts compared to
521 wild type plants. We propose that CML49 acts as general interactor together with the SAPs as
522 stress-specific partners. First, CML49 is constitutively expressed and SAP2 and SAP3 are
523 preferentially translated during H-light acclimation with the interaction of SAPs and CML49
524 resulting in relocation of the complex in the nucleus. Second, of the 215 transcripts downregulated
525 in *cml49* plants after 60 min of L→H-transfer a stress subset of 32 are downregulated in *sap3*.
526 Thus, the stress-responsive protein, SAP3, is providing specificity to what would be otherwise a
527 broader CML49 response (Figure 4 a). Cumulatively, the preferential translation of the SAPs and
528 their interaction with CML49 but also other TFs like DREB2A and HSF2A form a translation-
529 reliant signal pathway affecting nucleus transcription (Figure 5, II Translation-Reliant Nuclear
530 Circuit).

531 This translation-reliant nuclear circuit regulates two major clusters of genes. As noted above, the
532 majority of the transcripts regulated by the proposed CML49-SAP3 module code for stress

533 responsive transcripts. A subset which includes cytosolic *HSP70*, *HOP3*, *ROF2*, *HSFA2*, *HSP90.1*,
534 *HSP20-like* that increase after 1 h of L→H shift (Figure 4 a). Interestingly, *HSP90.1* and *ROF1*
535 interaction is needed for HSFA2-dependent heat memory and also regulates short HSPs (sHSPs)
536 (69). Of interest in this respect is our earlier report with Joanne Chory and colleagues of HSFs
537 translocation to the nucleus being redox-regulated (70). Taken together, we propose that this
538 mechanism forms a feed-forward loop that can amplify the transcriptional responses over time, the
539 translation-reliant retrograde stress signaling pathway (Figure 5, II. Translation-reliant Nuclear
540 Circuit).

541 A second subset of transcripts co-regulated by CML49 and SAP3 takes part in an acclimatory and
542 anterograde signaling pathway that collectively could contribute to chloroplast acclimation.
543 Among the transcripts were VTC2 encoding the GDP-L-galactose phosphorylase which catalyzes
544 the rate limiting enzymatic step in ascorbate synthesis (71). With respect to anterograde signaling,
545 plastidic sigma factor 5 (SIG5) is utilized by plastome-encoded RNA-polymerase (PEP) to
546 transcribe the plastidial psbD gene coding for the D2 protein of the reaction center of photosystem
547 II (5), which is known to be induced by H-light (72). SIG5 and D2 transcripts were increased in
548 response to the L→H-shifts, and SIG5 was reduced in the *cml49* and *sap3* knockouts, providing
549 evidence for an anterograde circuit altering chloroplast transcription in response to translational-
550 dependent retrograde signaling.

551 **Conclusion**

552 This work reveals a translation-dependent retrograde signaling pathway and identifies major
553 participants across key stages that regulate rapid stress acclimation responses after L→H-light
554 transfer. The translatome reorganization initiated by L→H involves a phosphorylation cascade,
555 that includes MPK6 and the AKIN10 subunit of SnRK1, which inhibit global translation and
556 preferential transcripts loading to the polysomes. This may serve as a very efficient local control
557 mechanism and possibly outcompetes transcriptional control in terms of time requirement needed
558 to initiate acclimation by just in time-provision of needed proteins to the plastids. The preferentially
559 loaded transcripts directly code for repair and photosynthesis-related proteins forming a direct
560 translational retrograde circuit (Figure 5). Translational efficiency is influenced by conserved
561 motifs in their 5'-UTR acting as RBP binding sites. The motifs, GAPC2 and ATP synthase subunit
562 alpha function in the direct circuit. In parallel, a translation-reliant nuclear circuit is activated to
563 increase nuclear expression of stress- and plastid-associated transcripts. In addition to known

564 transcription factors, SAP2 and SAP3 increase in response L→H and interact with the Ca^{2+} sensor
565 CML49 to promote accumulation of stress-responsive transcripts and anterograde signaling via
566 SIG5, which functions in plastid transcription. The elucidation of multiple components of a
567 bifurcating translation-dependent retrograde signaling pathway allows for rapid tuning of protein
568 synthesis to account for the demand of the photosynthesizing cell.

569 Materials and Methods

570 **Plant growth and treatments.** *Arabidopsis thaliana* wild-type (ecotype Columbia) and mutants
571 (*cml49-1* (SALK_090873), *cml49-2* (SALK_035905), *sap3-2 (SALK_022340), sap3-3*
572 *(SALK_136520C)*, *sap2-1* (SALK_008677), *sap2-2* (SAIL_1182_C11), *mpk6-3* (*73*), and *akin 10*
573 (GABI_579E09) were grown under short day conditions (10 h light with 80-100 µmol photons m^{-}
574 ^{2} s^{-1}, and 21°C/ 14 h dark, and 18°C, 50 % relative humidity) for three weeks prior to transfer to
575 8 µmol photons m^{-2} s^{-1} (L-light) for 10 days. Plants were transferred to 800 µmol photons m^{-2} s^{-1}
576 (H-light) for time periods as indicated, while control plants remained in L-light. Whole rosettes
577 were harvested under control and H-light conditions in the midday point of the light period to
578 exclude circadian effects and immediately frozen in liquid nitrogen and stored at -80°C.

579 **Sucrose cushion for polysome isolation.** Total ribosomes and ribosome-bound mRNA were
580 extracted and separated using sucrose gradient centrifugation as described (*74*). 3 g of pulverized
581 plant material was used with 6 mL polysomal extraction buffer (PEB; 0.2 M Tris, pH 9.0, 0.2 M
582 KCl, 25 mM EGTA, 35 mM MgCl, 1 % Brij, 1 % Triton X-100, 1 % Tween 20, 1 % Igepal CA630,
583 1% sodium deoxycholate (DOC), 1 % polyethylene-10-tridecylether (PTE), 5 mM DTT, 1 mM
584 PMSF, 100 µg/mL cycloheximide, 100 µg/mL chloramphenicol, 100 µg/mL lincomycin). The
585 suspension was passed twice through Miracloth™ and subsequently cleared by centrifugation.
586 Extracts were loaded on a sucrose cushion (0.2 M Tris, pH 9.0, 0.2 M KCl, 0.025 M EGTA,
587 0.035 M MgCl, 1.75 M sucrose, 5 mM DTT, 50 µg/mL cycloheximide, 50 µg/mL
588 chloramphenicol, 50 µg/mL lincomycin) and centrifuged for 18 h at 100,000 *x*g in a Beckmann
589 SW71Ti rotor. The sediment was suspended in 100 µL RNase digestion buffer (20 mM Tris-HCl,
590 pH 8.0, 140 mM KCl, 35 mM $MgCl_2$, 50 µg/µL cycloheximide, 50 µg/µL chloramphenicol,
591 50 µg/µL lincomycin) and used immediately for RNase I digestion.

592 **Polysomal mRNA and protein extraction**. Guanidinium chloride-precipitated polysomal
593 fractions were used for RNA isolation and subsequent cDNA synthesis as described in (*75*). For

594 protein isolation guanidinium chloride-precipitated polysomal fractions were pooled, proteins
595 extracted with pH-buffered phenol, precipitated with ethanol/NH_4 acetate and used for analysis in
596 denaturing polyacrylamide gel electrophoresis.

597 **RNase I digestion.** RNase I digest was performed with 2,000 relative absorbance units OD_{260} of
598 the in RNase digestion buffer suspended polysomes by adding 50 U of RNase If (New England
599 Biolabs) in 250 µL total volume by incubation at room temperature with constant rotation for 1 h.
600 In parallel same amounts of polysomes were treated with 5 µL SUPERase RNase inhibitor
601 (Thermo) and kept on ice as control sample. The digestion was stopped by adding 5 µL SUPERase
602 RNase inhibitor and the RNA precipitated by adding 1 volume of isopropanol, 300 mM NaOAc
603 pH 5.2 and 20 µg glycogen at -80 over-night. The supernatant was discarded after centrifugation
604 at 16,000 *x*g at 4 °C for 30 min and the sediment was washed twice with 75 % ethanol and
605 resuspended in RNA loading buffer for size exclusion electrophoresis.

606 **Library sequencing and analysis of mRNAs.** Total RNA was isolated using Tri Reagent (Sigma-
607 Aldrich) from extracts suspended in polysomal extraction buffer (see sucrose cushion for polysome
608 isolation, above). Briefly, 500 µL of extract was combined with 1 mL of TriReagent, followed
609 twice by extraction of the organic phase with 200 µL chloroform. RNA was precipitated with equal
610 volume 100% isopropanol and incubated overnight at -20°C. The RNA was recovered by
611 centrifugation and washed with 75% ethanol before resuspension in water. RNA quality was
612 assessed using a LabChip GXII (Perkin-Elmer). Total RNA was DNase-treated using TURBO
613 DNase (Invitrogen) following the manufacturer's protocol. Preparation of total RNAseq libraries
614 was carried out using Illumina TruSeq Stranded Total RNA with Ribo-Zero plant, scaled at half
615 reaction volumes.

616 Libraries of ribosome-protected fragments (RPFs) were prepared following RNase If digestion
617 (above) according to Juntawong et al. (2014) with minor modifications. RNA linker, rRNA
618 subtraction, and PCR oligonucleotides were ordered from Integrated DNA Technologies (IDT) and
619 are listed in Suppl. Table 2. Oligonucleotides for rRNA subtraction were adapted from those listed
620 in (*29*) and (*76*)

621 Total RNA and RPF sequencing libraries were quantified using the Qubit fluorometer (Invitrogen)
622 and size distribution was assessed using the LabChip GXII. Samples were pooled and sequenced

623 (75 bp single end) on the NextSeq500 at the Biomolecular Resource Facility (BRF) at the
624 Australian National University.

625 Quality control of sequencing data was performed with FastQC (v.0.11.5). Total RNA data had
626 adapters removed using scythe (v.0.991) with a prior of 0.01, and quality trimmed with sickle
627 (v.1.33) with a quality threshold of 20 and a minimum trimmed length of 20. Mapping to TAIR10
628 was performed with subjunc (v.1.4.5), reporting only reads with a single unambiguous mapping
629 location (*77*). RPF data was trimmed for adapter contamination and read quality using cutadapt
630 (v.1.9.1) with a minimum trimmed length of 20 bp and error rate of 0.1 (*78*). Trimmed reads were
631 mapped to TAIR10 using bowtie2 (v2.2.9) requiring end-to-end alignment and a substring length
632 of 10 (*79*). Total and RPF-mapped reads were summarised using featureCounts (*80*). Counts data
633 was converted to reads per kilobase million (RPKM) in R using edgeR (*81, 82*)

634 **TE calculation and transcript clustering.** Translation efficiency (TE) calculation followed
635 published protocols (*83*) as quotient of RPKM from RPF and RPKM from total RNA sequencing
636 for control and stress condition. The TE fold change (TE FC) was calculated as $TE_{stress}/TE_{control}$.
637 Cut-offs for DEGs were chosen according to upper and lower quantiles from a random distribution
638 analysis of all regulated polysome-associated and total transcripts (total mRNA: 1.5 and 0.75 and
639 polysomal: 1.1 and 0.75; 0.05 error margin). Clusters were derived for significantly transcripts
640 changed up and down in both polysomal and total RNA (cluster 1 and 4). Cluster 2 and 3 were
641 selected by filtering for only significantly up- and down-regulated in the polysomal set and not
642 significantly changed in total RNA and were termed preferential polysome-loaded transcripts
643 (PPLT) and preferential polysome-unloaded transcripts (PPUT).

644 **Whole genome ATH1 microarray.** Total RNA was isolated from 1 h L→H-light treated *sap3*,
645 *cml49* and WT *Arabidopsis* plants using RNeasy mini Kit (Qiagen). Controls were kept in L-light.
646 The hybridization of the Affymetrix ATH1 genome Array was commissioned to KFB (Regensburg,
647 Germany). Each condition was hybridized three times from independent experiments for *sap3* and
648 WT and once for *cml49*. Microarray data were analysed with ROBIN (MPI Golm, Potsdam,
649 Germany) and normalized with RMA algorithm (*84*). Transcripts were considered as differentially
650 regulated if the fold change was >2 and the adjusted *p*-value <0.05 (*85, 86*).

651 **Transcript profiling.** RNA isolation and cDNA synthesis were performed as in (*75*). Quantitative
652 real-time PCR (qPCR) of total and polysomal transcripts was conducted as described in (*28*) with

653 the difference of using KAPA SYBR® FAST qPCR Kit (Kapa Biosystems, South Africa). *Actin2*
654 (At3g18780) and *Tubulin5* (At1g20010) were used as reference genes.

655 **RNA electrophoretic mobility-shift assay (RNA-EMSA).** 5'-biotinylated RNA and unmodified
656 RNA of Motif 3 (5'-AAAUCGCCGGAG-3' 5'-BioTEG-AAAUCGCCGGAG-3') were
657 synthesized by Eurofins (Hamburg, Germany) and used for LightShift™ Chemiluminescent RNA
658 EMSA Kit (Thermo Scientific). Total protein was extracted from L-light and 10 min L→H-treated
659 plants using extraction buffer (25 mM Tris, pH 7.8, 75 mM NaCl, 15 mM EGTA, 15 mM
660 glycerophosphate, 15 mM 4-nitrophenyl pyrophosphate, 10 mM $MgCl_2$, 1 mM DTT, 1 mM NaF,
661 0.5 mM NA_3VO_4, 0.5 mM PMSF, 10 µg/mL leupeptin, 10 µg/mL aprotinin, 0.1 % Tween-20).
662 Prior to separation by non-denaturing polyacrylamide gel electrophoresis, RNAs were incubated
663 with extracts at room temperature for 30 min. Biotinylated RNA was detected by
664 chemiluminescence with streptavidin-HRP. For targeted EMSA AtGAPC1 and C2 were expressed
665 in *E.coli* BL21 (DE3) pLysS and purified as described in (*87*) with slight modifications. Buffers
666 were not supplemented with NAD^+ and purified protein was stored in 10 mM NaPi, pH 7.4.
667 AtGAPC1, AtGAPC2 and GAPDH from rabbit muscle (SIGMA Aldrich) were used for mobility
668 shift assays with 5'-biotinylated M1-RNA (5'-BioTEG-AUAUAUUCUCCGGAGAA-3'), 5'
669 biotinylated M2-RNA (5'-BioTEG-AUAUAUGAGAUUAGGGUUU-3') and 5'-biotinylated
670 SAP3 M1 (5'-Bio-ACCAGAUUUUUUUCGCCGGAGUUUGUUUUGAUCCA-3').

671 **Reporter gene construct and transient protoplast assay.** For the reporter gene construct assay
672 solely ubiquitin 10 5'-UTR as control (CCATGGCTTGATCACGGTAGAGAGAATTG–
673 AGAGAAAGTTTTTAAGATTTTGAGAAATTGAAATTCTCG) or ubiquitin 10 5'-UTR with
674 motifs (M1: CCATGGCTTGATCACGGTAGAGAGAATTGAGAGAAAGTTTTTTTC–
675 TCCGGAGATTCTCCGGAGATTCTCCGGAGAAAGATTTTGAGAAATTGAAATTCTCGA
676 G; M2: CCATGGCTTGATCACGGTAGAGAGAATTGAGAGAAAGTTTTTAAACCC–
677 TAATCTCAAACCCTAATCTCAAACCCTAATCTCAAGATTTTGAGAAATTGAAATTCTC
678 GAG; M3: CCATGGCTTGATCACGGTAGAGAGAATTGAGAGAAAGTTTTTCTCCGG–
679 CGACTCCGGCGACTCCGGCGAAAGATTTTGAGAAATTGAAATTCTCGAGA) were
680 cloned into MS129 luciferase reporter (*88*), and 5 µg plasmid DNA was co-transfected with same
681 amount of low-rate constitutively expressed pRL-TK *Renilla* luciferase vector (Promega) into
682 mesophyll protoplasts isolated from *A. thaliana* leaves by the downsized polyethylene glycol-
683 mediated transfection method (Seidel et al., 2004). After 12 h of acclimation half of the transfected

684 protoplasts were transferred to 800 µmol photons·m^{-2}·s^{-1} for 10 min and subsequently flash frozen
685 in $N_{2\ liq}$ for cell extracts. Luciferase activity of cell extracts was measured with Sirius L Tube
686 Luminometer (Berthold) and the luciferase assay system (Promega).

687 **RBP pulldown and identification.** Affinity pulldown with motif-carrying biotinylated RNA for
688 detection and identification of potential protein-RNA interactors was conducted as described in
689 (*89*) with minor differences. In short: 500 µg (or 250 µg for pull down followed by
690 immunodetection of cytosolic GAPDH) of total protein from L-light and L→H-treated plants were
691 incubated for 30 min at RT with 1 µg biotinylated M1- or M2-RNA (3 µg for 5'-Bio-*SAP3*-M1),
692 1 µL aprotinin (25 µg/µL), 1 µL leupeptin (25 µg/µL), 2 µL RNasin (Promega), 250 µL TENT
693 buffer (0.02 M Tris-HCl, pH 8.0), 0.002 M EDTA (pH 8.0), 0.5 M NaCl, 1 % (v/v) Triton X-100)
694 and adjusted to 500 µL with TENT buffer. 50 µL Dynabeads (Thermo Fisher) were added and
695 incubated under slow shaking for 30 min at RT. After precipitation and three washing steps with
696 TENT buffer, Dynabeads were dissolved in 1x protein loading buffer and incubated for 10 min at
697 95 °C, precipitated and the supernatant loaded on SDS-PAGE for separation and band
698 identification via mass-spectrometry or immunodetection of GAPC1/C2 after blotting the gel-
699 separated proteins on nitrocellulose membrane by semi dry electro blotting technique.

700 **Promotor and uORF analysis.** The +50 to -1000-bp region upstream of the ATG start codon and
701 +500 downstream of the transcription stop site of the CML49 and SAP3 co-regulated genes were
702 analysed for common *cis*-elements using PlantPAN2.0 (*90*). For uORF analysis the web tool
703 uPEPperoni was used (*91*) and the eFP Browser 2.0 for general expression pattern (*92*).

704 **mbSUS-analysis.** Vector construction of the mating-based Split-Ubiquitin-System analysis was
705 performed with the Gateway® cloning system (InvitrogenTM). The coding sequences of SAP2,
706 SAP3 and CML49 were fused to attB recombination sites and cloned into the pDONRTM221-
707 vector by a BP-reaction. Subsequently, each entry clone was used in a LR-reaction with the
708 destination vectors pX-NubWTgate (Nub) and pMetYCgate (Cub). Controls were the transformed
709 diploid yeast with NubI- (pNubWtX-gate, positive control) and the NubG-vector (pNX35-Dest,
710 negative control) as prey. The resulting vectors were transformed via lithium acetate transformation
711 into *Saccharomyces cerevisiae* strains THY.AP5 and THY.AP4, respectively (*93*). Yeast cells were
712 grown in 20 mL selective Nub/Cub medium at 30°C/140 rpm for 5-7 days. To start the mating step,
713 THY.AP5 and THY.AP4 were transferred to YPD plates and grown for 1 d at 30°C. For the
714 methionine assays, mated yeast was cultivated in selective liquid diploid medium for 3 d (30°C,

715 140 rpm). OD600 of selected yeast cells were measured and diluted to OD600 of 0.1 and 1.0
716 respectively in sterile water. Then 6 µL drops of each dilution were transferred to agar plates
717 containing no (Met 0 µM) or 0.075 % (v/v) methionine (Met 50 µM). Subsequently, the yeast was
718 grown for 72 h at 30°C and results documented photographically (*93, 94*).

719 **Subcellular localization and FRET measurements.** The coding sequences of the genes of interest
720 were fused in frame to yellow or cyan fluorescent protein as indicated and fluorescence resonance
721 energy transfer (FRET)-experiments were performed as described by (*95*) with CLSM 780 (Zeiss).
722 More than 20 protoplasts were measured twice for each set of PEG-based transformation and the
723 experiment was repeated independently

Acknowledgements

The authors acknowledge support by the Deutsche Forschungsgemeinschaft (Di 346/19; SP1935) and especially thank Diep Ganguly for discussion of statistics and data analysis and Renate Scheibe for providing the pET16b construct for recombinant expression of GapC1/C2.

The authors declare that they have no competing interests.

Data availability

All relevant data is accessible in this manuscript or in the supplemental material.

Authors contributions

MM designed the research and performed the polysomal gradients, transcript profiling, microarrays, RPF-seq and total RNAseq bioinformatic data analysis, transient protoplast reporter gene assays, RNA-EMSA, protein affinity pull downs and wrote the paper. AS did the RPF-library preparation and sequencing and performed bioinformatic analyses. CW prepared polysomal gradients and transcript profiling. SS performed Y2H experiments and cellular localization and FRET. MW performed RBP affinity pull downs and gel shift assays on SAP3 motifs. AF measured FRET and transcript profiles of OsSAP and OsCML49. TS supervised and performed FRET measurements. BP supervised and discussed the results and wrote the paper. KJD designed the study, supervised and discussed the results, coordinated the group and wrote the paper.

Figure legends

Figure 1: Ribosome loading and ribosomal profiles. (a) Lowlight (L)-acclimated plants were maintained in L-light (0‘) or transferred to Highlight (H, 10‘) and then transferred back to L for the indicated time (recovery). Ribosome-loading efficiency was determined by comparing mRNA quantity in ribosomal footprints to total mRNA (mean ± SE from n=3 independent experiments). Comparison of RPKM of 10 min L→H relative to L-light control. Letters indicate significance of difference as determined with ANOVA post-hoc Tukey $p<0.5$. (b) Comparison of translational efficiency (TE) of individual mRNAs under LL and HL. Also indicated are the numbers of transcripts with significantly higher or lower TE than average between LL and 10 min HL. (c) Change in total mRNA and translation efficiency for same genes as in (b). Quantiles were defined by random distribution analysis and set as cut-offs (TE: 1.41 and 0.74; total mRNA: 1.5 and 0.75; 0.05 error margin) for regulation of translation vs. transcription of all significant RPKM reads (FDR significance of $p<0.05$). (d) Significant changes in polysomal and total mRNA given as fold changes under LL and HL (cut-offs poly: 1.1 and 0.75; total mRNA 1.75 and 0.7; 0.05 error margin; FDR significance of $p<0.05$) with clustering into groups by polysomal and not significantly total mRNA changed (PPLT; red and PPUT; steel blue), polysomal and total mRNA changed (Poly and Total; blue) and only total changed without significantly changed polysomal transcripts (buffered; salmon).

Figure 2: Identification and functional validation of three motifs in the 5’UTR of preferentially polysome-loaded transcripts. These motifs are hypothesized to confer preferential translation after 10 min L→H. (a) In 338 5’-UTRs of the preferentially loaded transcripts specific motifs were detected using the MEME algorithm against a randomized 5’-UTR set. Motifs 1 and 3 were present in 32% of those transcripts, and motif 2 in 13% with an additional 8% occurrence in their respective 3’ UTR. (b) Schematics of constructs used in the reporter assays. The 5’-UTR of ubiquitin 10 was cloned upstream of the luciferase (LUC) reporter under control of the ubiquitin promotor. Triplet motifs were introduced into the 5’-UTR of ubiquitin mRNA. *A. thaliana* mesophyll protoplasts were co-transfected with one of each construct and with the pGL4::RLUC reference construct. (c) Relative LUC signal in lysed mesophyll protoplasts treated with H-light for 10’ normalized to reference construct. The construct containing M1 showed a strong increase in LUC signal after L→H. Data are means ± SD from two independent experiments with 10 replicates, * and + indicate significant difference to ubiquitin control, two sided Student’s t-test: $p<0.05$ and 0.1 , respectively.

Figure 3: Interaction of SAP2 or SAP3 with CML49 in the split-ubiquitin yeast-two-hybrid system and by Förster resonance energy transfer (FRET) of SAP2:CFP or SAP3:CFP with CML49:YFP in *A. thaliana* protoplasts. (a) Quantification of interaction strength between SAP2 or SAP3 and CML49 using a methionine-dependent split-ubiquitin-assay. Depicted are colonies after 72 h at 30 °C in different ODs (OD = 0.1 and 1.0). Growth was monitored either on Met 0 µM (no methionine, left colonies) and Met 50 µM (50 µM methionine, right colonies) medium plates. Diploid yeast was transformed with NubI- (pNubWtX-gate) as positive control and as negative control with the NubG-vector (pNX35-Dest) as prey (depicted are representative images of n=3 independent experiments). (b) *A. thaliana* mesophyll protoplasts were transfected with SAP2:CFP, SAP3:CFP or CML49:YFP vector DNA. Fluorescence images taken by CLSM for subcellular localization. Following transfection with SAP2:CFP or SAP3:CFP and CML49:YFP constructs, FRET efficiencies between CFP and YFP were quantified. FRET was also determined with CFP:YFP as positive control and 35S::CFP with 35S::YFP as negative control (for each set of transformation > 20 protoplast were measured twice with n=3 independent experiments).

Figure 4. Deregulated H-light response in *sap3* and *cml49* compared to WT. (a) Microarrays were hybridized with cDNA from WT, *cml49* and *sap3* after 60 min of L→H transfer. Assuming a concerted function of SAP2 and SAP3 together with CML49 in the H-light response, the data were filtered for co-regulated targets that are stronger deregulated in *cml49* than *sap3* background. The expression level corresponds to the colour intensity with yellow = -1 and blue = 5 (log_2 fold). (b-f) Validation of transcript responses to H-light of putative CML49 and SAP3 targets. VTC2, HSP20-like, PS3, SIG5 and eEF1B were selected based on the transcriptome response, and their transcript levels quantified by qPCR following the L→H-transfer. Data are means ± S.D. of n=4 independent experiments, asterisks indicate significant difference, two sided Student's t-test $p<0.05$.

Figure 5: Schematics of translation-dependent retrograde signalling (TraDeRS). Rapid regulation of polysome loading and unloading after 10 min of L→H shift was partially disturbed in *mpk6* and *akin10* mutants indicating retrograde regulation of translation. Regulation involves transcription-independent changes of translational efficiency of majorly chloroplast targeted proteins involved in photosynthesis as well as chloroplast-associated assembly, repair and import of proteins, thus forming a direct feedback circuit regulated via translation (I. Direct Translational Circuit). The preferential loading of key transcription factors as well as *SAP2* and *SAP3* are part of the translation-reliant synchronization of the nucleus with the changed chloroplast demand (II. Translation-Reliant Nuclear Circuit). SAP2 and SAP3 interact with CML49 and this regulatory module affects transcript abundance of, e.g. VTC2 and SIG5, participating in anterograde signalling, and other major stress response genes like ANAC2, HSP101 and HOP3.

Supplementary materials

Suppl. Fig. 1: Preferential loading of selected transcripts after 10 min L→H transfer and deregulation in *akin10*. (a-e) Five transcripts were selected from the transcriptome data set and subjected to qPCR analysis in wildtype (WT) and *akin10*. SAP2 and SAP3 showed significantly higher polysome association after L→H-transfer for 10 min. (Data are means ± SE of n=3 independent experiments, * indicate significance difference relative to control, two sided Student‘s t-test: $p < 0.05$, 0.1, respectively). (f-h) Absorbance (A254 nm) of sucrose density gradient of WT, *mpk6* and *akin10* treated with L-Light (control) and L→H transfer for 10 min (depicted are representative profiles of n=3 replicates).

Suppl. Fig. 2: Distribution and secondary structure of motif-carrying 5‘UTRs. (a) Motif 1, 2 and 3 occurrences in their respective transcripts as revealed by MEME-suit. (b) The secondary structure is given in Dot-Bracket notation and was calculated using the software *RNA Shapes Studio (96)*, with Motifs drawn at corresponding site(s) for motif 1 (green), 2 (yellow) and 3 (red), respectively. (c) Distribution of motif-carrying transcripts in translatomes are indicated as dots for transcripts carrying motif 1 (green), 2 (yellow) or 3 (red). (d) Relative ribosomal loading (HL/LL) of motif-carrying transcripts (M1 – M3) and all translationally regulated transcripts with (All Transcripts) and without motifs (All Other Transcripts).

Suppl. Fig. 3: Motifs are possible RBP binding sites. (a) 5‘-biotinylated M3-RNA with and without unlabelled competitor M3-RNA was incubated with total protein extracts of L-light or 10 min L→H shifted plants, respectively. Depicted is a representative blot. (b,c) mRNP 1-D acrylamide gel. Biotinylated M1 and M2 RNAs were coupled to strep-tagged beads and incubated with protein extracts from LL and 10 min L→H treated plants. After washing, samples were eluted and loaded on one dimensional acrylamide gels. The indicated bands were cut out and analysed via MALDI. (d) Best Mascot scores for indicated bands from b & c. (e) RNA-EMSA was used to validate interaction of M1- and M2-RNA with Arabidopsis cytosolic GAPDH isoform C1 *in vitro*. (f) Immunodetection of AtGapC1/C2 after RNA-based affinity pull down with native M1 from *SAP3* 5’-UTR as described for M1 and M2 in b & c. Elution: eluted proteins associated with the RNA-functionalized beads, FT: Flow through, supernatant after affinity pull down, Input: Plant extract prior to affinity pull down. (g-i) RNA-EMSA performed with 5’-Bio *SAP3*-M1 and AtGapC2 (g), AtGapC1 (h) or GAPDH isolated from rabbit muscle (i).

Suppl. Fig. 4: Representation of motifs 1-3 from *A. thaliana* as Hidden Markow Models and comparison with related motifs in rice SAP8 and SAP9. OsSAP8 and OsSAP9 were identified as closest homologues of SAP2 and SAP3 from *A. thaliana*. Each motif could be identified in the 5’-and 3’-UTR of the rice homologues with slight variation.

Suppl. Fig. 5: Gene expression map and polysome loading of *OsSAP8, OsSAP9* and *OsCML49a*. (a) Transcript abundance of *SAP8*, (b) *SAP9* and (c) *CML49a* in different rice tissues retrieved from the Rice eFP Browser. *CML49b* was missing in group 1 data source of Rice eFP Browser. (d,e) qPCR-based quantification of *OsSAP8* and *OsSAP9* transcripts in total and polysomal RNA fractions after 10 min of L→H-transfer. Data sets were normalized to *Actin* and *α-Tubulin* and represent means ± SD of n=2 independent experiments, asterisks indicate significance relative to control, two sided Student's t-test: $p < 0.05$.

Suppl. Fig. 6: Subcellular localization of rice OsSAP8, OsSAP9, OsCML49a and OsSAP49b in transfected Arabidopsis protoplasts and their molecular interaction shown by FRET. *A. thaliana* mesophyll protoplasts were transfected with OsSA8:YFP, OsSAP3:YFP, OsCML49b:CFP or OsCML49a:CFP vector DNA. Fluorescence images taken by CLSM for subcellular localization. Following transfection with constructs, FRET efficiencies between CFP and YFP were quantified.

Suppl. Table 1. Translation efficiency (TE) of selected transcripts in *mpk6* and *akin10* background. Target transcripts were quantified in total and polysomal mRNA via qPCR (Suppl. Fig. 1.). Two transcripts were selected for their increase in TE (*SAP2* and *SAP3*) and three for their decrease in TE (*ERF105*, *DREB2A*, *HSP70*). (TE was calculated from n=3 independent experiments, asterisks indicates significant difference $p<0.05$; ANOVA)

TE	TE increased		TE decreased		
Name	SAP2	SAP3	ERF105	DREB2A	HSP70
WT	6.1	2.6	0.4	0.2	0.07
mpk6	1.2*	1	0.3	0.4	0.26*
akin10	1.8*	0.6	1.1*	1.2*	0.58*

Suppl. Table 2. Oligonucleotides.

Target gene	ID number	Forward Sequence (5'–3')	Reverse Sequence (5' – 3')
HSP20-like	AT1G53540	GTTCGAAGGTTTCTTGACGC	TGTCTCCCTCCAATCCACTT
HSP70	AT3G12580	TCGACTGCTCAGACGACTAT	GAACCTAGCACGAGTGATGG
SAP2	AT1G51200	TGAGCCGATGACTGTTTCTG	TTGGTTTCGCAGCTTCTTCT
SAP3	AT2G27580	GGTGTGGTTTCGTTTTCTGC	GCTTTCACAATCGGATTCGC
VTC2	AT4G26850	GACTGCTGTGTTTGCCTTCA	CGGGCTCACTTCACCTAGAG
eEF1B	AT5G12110	ATCTCCACACAGAGCGAGGT	TTGCTAGCATTGGGAAAACC
SIG5	AT5G24120	TCCTCCTCGTGAGCAAGTTT	GGAGCCGAATTATGTTCCAA
PS3	AT3G47420	TTGGTTAACGGTCCTTACGC	CGTTACCGTAGCCAAAGCTC
OsSAP8	Os06G41010	CGATGTGGCAACTTGTACTG	TTAGCCTTGGCAATAGCATC
OsSAP9	Os07G07350	AAACAACTGTGGCTTCTTCG	CGTAAATGCCTTCTTCTCCA
OsActin	Os03G07181	AGGCCGTCCTCTCTCTGTAT	GGGGAGAGCATATCCTTCAT
Osα-tubulin	Os03G51600	TCTGAACGTGGATGTCAATG	GAGATCACTGGAGCGTAGGA
OsSAP8NotI		AAAAGCGGCCGCATGGAGCACAAGGAGACT	
OsSAP8EcoRI		TTTTGAATTCCTAAATTTTGTCAAGTTT	
OsSAP9NotI		AAAAGCGGCCGCATGGCACAAGAAAGCTGG	
OsSAP9EcoRI		TTTTGAATTCTCAGATCTTGTTGATCTT	
OsCML49NotI		AAAAGCGGCCGCATGGCCGGCTACCCGCCA	
OsCML49EcoRI		TTTTGAATTCTTATGCAATGAGAAAAGG	
rRNA depletion	rRNA1b	CAGCTGAGGCATCCTAACAGACCGGTAGACTTG	
rRNA depletion	rRNA21	AGTAAGCCCACCCCAAGATGAGTGCTCTC	
rRNA depletion	rRNA27	ACGACTCTCGGCAACGGATATCTCGGCTCTCGCATCGATGAAGAACG	
rRNA depletion	rRNA29	GGCCGAGGGCACGTCTGCCTGGGTGTCAC	
rRNA depletion	rRNA30	GACTGTGAAACTGCGAATGGCTCATTAA	
rRNA depletion	rRNA44	TAGCGACGTTGCTTTTTGATCCTTCG	
rRNA depletion	rRNA1c	GATAACCGTAGTAATTCTAGAG	
rRNA depletion	rRNA1	CATAAACGATGCCGACCAGGGATCAGCGG	
rRNA depletion	rRNA2	TTTATTAGATAAAAGGTCGACG	

Suppl. Table 3: Overview of *cis*-elements within the promoter regions of CML49 and SAP3 co-regulated genes. The total number and type of *cis*-elements within the co-regulated subgroup was searched -1.000 bp upstream of the ATG region using PlantPAN2.0. The largest group of *cis*-elements belong to the WRKY-group, followed by MYB, MYB-related, SURE (sulfur-responsive element) and ABRE-like (early responsive to dehydration). Only few putative sites belong to the LS7 (salicylic acid-inducible element), C-box (bZIP factors), PHR1 (phosphate starvation response) and some represent cis-elements for light-dependent SORLIPs (Sequences Over-Represented in Light-Induced Promoters).

AGI	Name	MYB/ MYB-related	WBOX	SURE	PHR1	C-box	ABRElike	LS7	SORLIPs	Other
AT4G13800	unknown	29	37	35	4	2	20	4	17	24
AT5G52570	BETA-OHASE 2	24	36	29	6	2	27	4	30	26
AT5G49480	CP1	24	41	30	1	2	16	1	19	21
AT4G04020	FIB	22	39	18	5	3	19	3	26	16
AT5G58770	CPT4	35	35	22	3		23	3	30	29
AT3G56290	unknown	23	47	31	3	2	25	3	35	34
AT1G67360	REF	41	46	32	5	8	30	6	27	14
AT1G61800	GPT2	28	36	23	7	9	18	3	17	26
AT5G20150	SPX1	22	42	20	13	4	14	1	10	23
AT3G21890	BBX31	22	41	27	2	6	22	3	14	30
AT2G46830	CCA1	31	43	47	1	6	21	1	44	14
AT5G52640	HSP90.1	35	38	43	4	4	23	3	15	14
AT2G36800	DOGT1	32	48	44	5	6	28	3	30	14
AT5G48570	ROF2	24	49	30	2	4	22	1	15	14
AT1G52690	LEA7	27	44	27	5	8	32	4	28	25
AT2G24540	AFR	28	45	41	6	9	28	4	28	31
AT3G09350	Fes1A	34	41	40	3	9	26	9	25	21
AT4G21990	APR3	22	40	26	3	6	21	1	16	20
AT4G12400	HOP3	33	37	25	3	1	24	6	12	21
AT5G50800	ATSWEET13	26	43	32	4	7	24	5	30	19
AT2G37180	RD28	23	43	21	7	4	22	3	20	34
AT4G34550	PCH1-like	26	35	30	4	3	16	3	19	34
AT3G17609	HYH	27	38	27	6	5	24	3	28	30
AT5G64510	TIN1	34	44	34	4	12	27	9	30	30
AT1G01520	ASG4	33	34	45	3	2	29	7	38	26
AT1G32900	GBSS1	31	52	31	5	9	28	2	36	30
AT2G26150	HSFA2	20	60	46	0	4	19	3	30	34
AT5G12110	eEF1B	41	53	34	2	6	17	4	32	31
AT4G26850	VTC2	20	40	31	8	8	23	4	20	36
AT2G33380	RD20	29	42	26	6	7	38	3	22	29
AT3G21150	BBX32	26	41	39	5	6	17	5	30	23
AT3G09450	unknown	38	34	42	6	1	29	3	43	29
AT2G21320	BBX18	26	57	40	7	4	20	1	20	27
AT1G58520	RXW8	20	28	26	2	3	17	4	18	45
AT5G24120	SIG5	14	52	31	1	4	22	1	16	25
AT5G65380	MATE	24	47	31	4	8	32	7	33	29
AT3G53830	RCC1	24	40	35	6	4	31	2	18	27
AT3G17790	PAP17	37	44	34	7	8	28	6	31	29
AT1G54050	HSP20-like	44	40	30	6	5	15	3	38	31
AT1G62180	ATAPR2	29	53	24	5	3	26	3	27	28
AT3G21670	ATNPF6.4	22	44	27	3	1	25	2	21	37
AT3G12580	HSP70	20	42	24	4	1	18	2	11	32
AT2G46790	PRR9	22	43	26	6	3	19	1	44	33
AT1G77450	NAC032	31	45	35	4	6	33	8	35	30
AT2G15020	unknown	20	34	26	5	0	24	3	34	36
AT3G47420	PS3	30	42	10	7	2	21	5	18	27
AT5G63130	Phox/Bem1p	20	49	19	4	5	15	3	31	37
AT1G01720	ANAC2	29	39	50	2	6	22	2	36	23
AT4G26150	CGA1	26	34	27	5	2	15	2	14	36
AT1G74310	HSP101	20	35	33	5	2	13	1	17	34
	Total	1368	2112	1556	224	232	1148	173	1278	1368

Suppl. Table 4. uORF analysis of motif-carrying transcripts. The motif-carrying transcripts were screened for upstream open reading frames (uORF) coding for upstream peptides (uPEPs) using the online tool uPEPperoni.

Target gene	ID number	uPEPs Sequence (5'–3')	Position (start-end)
PHT3	AT2G17270	MRTLPTYTLFAFPFIAFL	(182, 235)
Methyltransferase superfamily protein	AT3G13440	MGLGRNLQTIRSSYKIRVF	(23, 79)
PDX1.2	AT3G16050	MEAHLVSFFCIRRRFAIPP	(14, 70)
RBL14	AT3G17611	MRVKRRSLWRICFRRDQAAAI	(8, 70)
Unknown protein	AT4G27010	MPDFELSASPICFVLLNPKTKTPRREKSSL	(53, 142)
HSFB1	AT4G36990	MEETKRNSDLLRSRVFLSGFYCWDWE	(267, 344)
SIG5	AT5G4088	MMMPSSSCFHFGLRFFISSIRDPPIRIDTQR SRVSTDMDMDKS	(159, 287)

References:

1. J. Barber, B. Andersson, Too much of a good thing: light can be bad for photosynthesis. *Trends in Biochemical Sciences* **17**, 61-66 (1992).
2. K. K. Niyogi, Safety valves for photosynthesis. *Current Opinion in Plant Biology* **3**, 455-460 (2000).
3. M. Baier, K. J. Dietz, Chloroplasts as source and target of cellular redox regulation: a discussion on chloroplast redox signals in the context of plant physiology. *J Exp Bot* **56**, 1449-1462 (2005).
4. K. Asada, THE WATER-WATER CYCLE IN CHLOROPLASTS: Scavenging of Active Oxygens and Dissipation of Excess Photons. *Annu Rev Plant Physiol Plant Mol Biol* **50**, 601-639 (1999).
5. A. Nagashima, The Multiple-Stress Responsive Plastid Sigma Factor, SIG5, Directs Activation of the psbD Blue Light-Responsive Promoter (BLRP) in Arabidopsis thaliana. *Plant and Cell Physiology* **45**, 357-368 (2004).
6. B. J. Pogson, N. S. Woo, B. Forster, I. D. Small, Plastid signalling to the nucleus and beyond. *Trends Plant Sci* **13**, 602-609 (2008).
7. J. Pfalz, T. Pfannschmidt, Essential nucleoid proteins in early chloroplast development. *Trends Plant Sci* **18**, 186-194 (2013).
8. T. Pfannschmidt, A. Nilsson, J. F. Allen, Photosynthetic control of chloroplast gene expression. *Nature* **397**, 625-628 (1999).
9. C. F. Beck, Signaling pathways from the chloroplast to the nucleus. *Planta* **222**, 743-756 (2005).
10. S. Koussevitzky, A. Nott, T. C. Mockler, F. Hong, G. Sachetto-Martins, M. Surpin, J. Lim, R. Mittler, J. Chory, Signals from chloroplasts converge to regulate nuclear gene expression. *Science* **316**, 715-719 (2007).
11. G. M. Estavillo, P. A. Crisp, W. Pornsiriwong, M. Wirtz, D. Collinge, C. Carrie, E. Giraud, J. Whelan, P. David, H. Javot, C. Brearley, R. Hell, E. Marin, B. J. Pogson, Evidence for a SAL1-PAP chloroplast retrograde pathway that functions in drought and high light signaling in Arabidopsis. *Plant Cell* **23**, 3992-4012 (2011).
12. Y. Xiao, T. Savchenko, E. E. Baidoo, W. E. Chehab, D. M. Hayden, V. Tolstikov, J. A. Corwin, D. J. Kliebenstein, J. D. Keasling, K. Dehesh, Retrograde signaling by the plastidial metabolite MEcPP regulates expression of nuclear stress-response genes. *Cell* **149**, 1525-1535 (2012).
13. S. W. Park, W. Li, A. Viehhauser, B. He, S. Kim, A. K. Nilsson, M. X. Andersson, J. D. Kittle, M. M. Ambavaram, S. Luan, A. R. Esker, D. Tholl, D. Cimini, M. Ellerstrom, G. Coaker, T. K. Mitchell, A. Pereira, K. J. Dietz, C. B. Lawrence, Cyclophilin 20-3 relays a 12-oxo-phytodienoic acid signal during stress responsive regulation of cellular redox homeostasis. *Proc Natl Acad Sci U S A* **110**, 9559-9564 (2013).
14. K. J. Dietz, Redox regulation of transcription factors in plant stress acclimation and development. *Antioxid Redox Signal* **21**, 1356-1372 (2014).
15. R. E. Häusler, L. Heinrichs, J. Schmitz, U. I. Flugge, How sugars might coordinate chloroplast and nuclear gene expression during acclimation to high light intensities. *Mol Plant* **7**, 1121-1137 (2014).
16. M. O. Vogel, M. Moore, K. Konig, P. Pecher, K. Alsharafa, J. Lee, K. J. Dietz, Fast retrograde signaling in response to high light involves metabolite export, MITOGEN-

ACTIVATED PROTEIN KINASE6, and AP2/ERF transcription factors in Arabidopsis. *Plant Cell* **26**, 1151-1165 (2014).

17. J. Schmitz, L. Heinrichs, F. Scossa, A. R. Fernie, M. L. Oelze, K. J. Dietz, M. Rothbart, B. Grimm, U. I. Flugge, R. E. Hausler, The essential role of sugar metabolism in the acclimation response of Arabidopsis thaliana to high light intensities. *Journal of Experimental Botany* **65**, 1619-1636 (2014).
18. P. A. Crisp, D. Ganguly, A. B. Smith, K. D. Murray, G. M. Estavillo, I. R. Searle, E. Ford, O. Bogdanovic, R. Lister, J. O. Borevitz, S. R. Eichten, B. J. Pogson, Rapid recovery gene downregulation during excess-light stress and recovery in Arabidopsis. *Plant Cell*, (2017).
19. G. Z. Wu, E. H. Meyer, A. S. Richter, M. Schuster, Q. Ling, M. A. Schottler, D. Walther, R. Zoschke, B. Grimm, R. P. Jarvis, R. Bock, Control of retrograde signalling by protein import and cytosolic folding stress. *Nat Plants* **5**, 525-538 (2019).
20. M. Moore, N. Gossmann, K. J. Dietz, Redox Regulation of Cytosolic Translation in Plants. *Trends Plant Sci* **21**, 388-397 (2016).
21. A. Lokdarshi, J. Guan, R. A. Urquidi-Camacho, S. K. Cho, P. W. Morgan, M. Leonard, M. Shimono, B. Day, A. G. von Arnim, Light Activates the Translational Regulatory Kinase GCN2 via Reactive Oxygen Species Emanating from the Chloroplast. *Plant Cell*, (2020).
22. M. Piques, W. X. Schulze, M. Hohne, B. Usadel, Y. Gibon, J. Rohwer, M. Stitt, Ribosome and transcript copy numbers, polysome occupancy and enzyme dynamics in Arabidopsis. *Mol Syst Biol* **5**, 314 (2009).
23. P. Juntawong, J. Bailey-Serres, Dynamic Light Regulation of Translation Status in Arabidopsis thaliana. *Front Plant Sci* **3**, 66 (2012).
24. J. Shin, A. Sanchez-Villarreal, A. M. Davis, S. X. Du, K. W. Berendzen, C. Koncz, Z. Ding, C. Li, S. J. Davis, The metabolic sensor AKIN10 modulates the Arabidopsis circadian clock in a light-dependent manner. *Plant Cell Environ* **40**, 997-1008 (2017).
25. C. Robaglia, M. Thomas, C. Meyer, Sensing nutrient and energy status by SnRK1 and TOR kinases. *Curr Opin Plant Biol* **15**, 301-307 (2012).
26. M. Nietzsche, R. Landgraf, T. Tohge, F. Börnke, A protein–protein interaction network linking the energy-sensor kinase SnRK1 to multiple signaling pathways in Arabidopsis thaliana. *Current Plant Biology* **5**, 36-44 (2016).
27. E. Baena-Gonzalez, F. Rolland, J. M. Thevelein, J. Sheen, A central integrator of transcription networks in plant stress and energy signalling. *Nature* **448**, 938-942 (2007).
28. M. L. Oelze, M. O. Vogel, K. Alsharafa, U. Kahmann, A. Viehhauser, V. G. Maurino, K. J. Dietz, Efficient acclimation of the chloroplast antioxidant defence of Arabidopsis thaliana leaves in response to a 10- or 100-fold light increment and the possible involvement of retrograde signals. *J Exp Bot* **63**, 1297-1313 (2012).
29. P. Juntawong, T. Girke, J. Bazin, J. Bailey-Serres, Translational dynamics revealed by genome-wide profiling of ribosome footprints in Arabidopsis. *Proc Natl Acad Sci U S A* **111**, E203-212 (2014).
30. M. O. Vogel, M. Moore, K. Konig, P. Pecher, K. Alsharafa, J. Lee, K. J. Dietz, Fast Retrograde Signaling in Response to High Light Involves Metabolite Export, MITOGEN-ACTIVATED PROTEIN KINASE6, and AP2/ERF Transcription Factors in Arabidopsis. *Plant Cell* **26**, 1151-1165 (2014).
31. C. M. Hooper, I. R. Castleden, S. K. Tanz, N. Aryamanesh, A. H. Millar, SUBA4: the interactive data analysis centre for Arabidopsis subcellular protein locations. *Nucleic Acids Res* **45**, D1064-D1074 (2017).

32. T. L. Bailey, C. Elkan, Fitting a mixture model by expectation maximization to discover motifs in biopolymers. *Proceedings of the Second International Conference on Intelligent Systems for Molecular Biology*, 28-36 (1994).
33. M. J. Liu, S. H. Wu, H. M. Chen, S. H. Wu, Widespread translational control contributes to the regulation of Arabidopsis photomorphogenesis. *Mol Syst Biol* **8**, 566 (2012).
34. S. Vij, A. K. Tyagi, Genome-wide analysis of the stress associated protein (SAP) gene family containing A20/AN1 zinc-finger(s) in rice and their phylogenetic relationship with Arabidopsis. *Mol Genet Genomics* **276**, 565-575 (2006).
35. F. Wang, R. A. Coe, S. Karki, S. Wanchana, V. Thakur, A. Henry, H. C. Lin, J. Huang, S. Peng, W. P. Quick, Overexpression of OsSAP16 Regulates Photosynthesis and the Expression of a Broad Range of Stress Response Genes in Rice (Oryza sativa L.). *PLoS One* **11**, e0157244 (2016).
36. A. Mukhopadhyay, S. Vij, A. K. Tyagi, Overexpression of a zinc-finger protein gene from rice confers tolerance to cold, dehydration, and salt stress in transgenic tobacco. *Proc Natl Acad Sci U S A* **101**, 6309-6314 (2004).
37. S. Yamasaki, A. Suzuki, Y. Yamano, H. Kawabe, D. Ueno, T. Demura, K. Kato, Identification of 5'-untranslated regions that function as effective translational enhancers in monocotyledonous plant cells using a novel method of genome-wide analysis. *Plant Biotechnol (Tokyo)* **35**, 365-373 (2018).
38. A. Nishizawa, Y. Yabuta, E. Yoshida, T. Maruta, K. Yoshimura, S. Shigeoka, Arabidopsis heat shock transcription factor A2 as a key regulator in response to several types of environmental stress. *Plant J* **48**, 535-547 (2006).
39. E. Stroher, X. J. Wang, N. Roloff, P. Klein, A. Husemann, K. J. Dietz, Redox-dependent regulation of the stress-induced zinc-finger protein SAP12 in Arabidopsis thaliana. *Mol Plant* **2**, 357-367 (2009).
40. F. Ferre, P. Clote, DiANNA: a web server for disulfide connectivity prediction. *Nucleic Acids Res* **33**, W230-232 (2005).
41. Y. Nishiyama, S. I. Allakhverdiev, N. Murata, Protein synthesis is the primary target of reactive oxygen species in the photoinhibition of photosystem II. *Physiol Plant* **142**, 35-46 (2011).
42. F. E. Belbin, Z. B. Noordally, S. J. Wetherill, K. A. Atkins, K. A. Franklin, A. N. Dodd, Integration of light and circadian signals that regulate chloroplast transcription by a nuclear-encoded sigma factor. *New Phytol*, (2016).
43. K. K. Niyogi, PHOTOPROTECTION REVISITED: Genetic and Molecular Approaches. *Annu Rev Plant Physiol Plant Mol Biol* **50**, 333-359 (1999).
44. I. Hebbelmann, J. Selinski, C. Wehmeyer, T. Goss, I. Voss, P. Mulo, S. Kangasjarvi, E. M. Aro, M. L. Oelze, K. J. Dietz, A. Nunes-Nesi, P. T. Do, A. R. Fernie, S. K. Talla, A. S. Raghavendra, V. Linke, R. Scheibe, Multiple strategies to prevent oxidative stress in Arabidopsis plants lacking the malate valve enzyme NADP-malate dehydrogenase. *J Exp Bot* **63**, 1445-1459 (2012).
45. M. L. Oelze, A. Kandlbinder, K. J. Dietz, Redox regulation and overreduction control in the photosynthesizing cell: complexity in redox regulatory networks. *Biochim Biophys Acta* **1780**, 1261-1272 (2008).
46. K. J. Dietz, M. O. Vogel, A. Viehhauser, AP2/EREBP transcription factors are part of gene regulatory networks and integrate metabolic, hormonal and environmental signals in stress acclimation and retrograde signalling. *Protoplasma* **245**, 3-14 (2010).
47. K. S. Browning, J. Bailey-Serres, Mechanism of cytoplasmic mRNA translation. *Arabidopsis Book* **13**, e0176 (2015).

48. Y. Zhang, Y. Wang, K. Kanyuka, M. A. Parry, S. J. Powers, N. G. Halford, GCN2-dependent phosphorylation of eukaryotic translation initiation factor-2alpha in Arabidopsis. *J Exp Bot* **59**, 3131-3141 (2008).
49. R. C. Wek, H. Y. Jiang, T. G. Anthony, Coping with stress: eIF2 kinases and translational control. *Biochemical Society Transactions* **34**, 7-11 (2006).
50. M. J. Clemens, A. Elia, S. J. Morley, Requirement for the eIF4E binding proteins for the synergistic down-regulation of protein synthesis by hypertonic conditions and mTOR inhibition. *PLoS One* **8**, e71138 (2013).
51. J. D. Richter, N. Sonenberg, Regulation of cap-dependent translation by eIF4E inhibitory proteins. *Nature* **433**, 477-480 (2005).
52. A. N. Bruns, S. Li, G. Mohannath, D. M. Bisaro, Phosphorylation of Arabidopsis eIF4E and eIFiso4E by SnRK1 Inhibits Translation. *FEBS J*, (2019).
53. J. B. Rossel, I. W. Wilson, B. J. Pogson, Global changes in gene expression in response to high light in Arabidopsis. *Plant Physiol* **130**, 1109-1120 (2002).
54. N. Suzuki, H. Sejima, R. Tam, K. Schlauch, R. Mittler, Identification of the MBF1 heat-response regulon of Arabidopsis thaliana. *Plant J* **66**, 844-851 (2011).
55. C. Branco-Price, K. A. Kaiser, C. J. Jang, C. K. Larive, J. Bailey-Serres, Selective mRNA translation coordinates energetic and metabolic adjustments to cellular oxygen deprivation and reoxygenation in Arabidopsis thaliana. *Plant J* **56**, 743-755 (2008).
56. C. H. Chang, J. D. Curtis, L. B. Maggi, Jr., B. Faubert, A. V. Villarino, D. O'Sullivan, S. C. Huang, G. J. van der Windt, J. Blagih, J. Qiu, J. D. Weber, E. J. Pearce, R. G. Jones, E. L. Pearce, Posttranscriptional control of T cell effector function by aerobic glycolysis. *Cell* **153**, 1239-1251 (2013).
57. M. R. White, E. D. Garcin, The sweet side of RNA regulation: glyceraldehyde-3-phosphate dehydrogenase as a noncanonical RNA-binding protein. *Wiley Interdiscip Rev RNA* **7**, 53-70 (2016).
58. C. Marondedze, L. Thomas, C. Gehring, K. S. Lilley, Changes in the Arabidopsis RNA-binding proteome reveal novel stress response mechanisms. *BMC Plant Biol* **19**, 139 (2019).
59. J. Giri, S. Vij, P. K. Dansana, A. K. Tyagi, Rice A20/AN1 zinc-finger containing stress-associated proteins (SAP1/11) and a receptor-like cytoplasmic kinase (OsRLCK253) interact via A20 zinc-finger and confer abiotic stress tolerance in transgenic Arabidopsis plants. *New Phytol* **191**, 721-732 (2011).
60. M. Kang, M. Fokar, H. Abdelmageed, R. D. Allen, Arabidopsis SAP5 functions as a positive regulator of stress responses and exhibits E3 ubiquitin ligase activity. *Plant Mol Biol* **75**, 451-466 (2011).
61. G. D. Kim, Y. H. Cho, S. D. Yoo, Regulatory functions of evolutionarily conserved AN1/A20-like Zinc finger family proteins in Arabidopsis stress responses under high temperature. *Biochem Biophys Res Commun* **457**, 213-220 (2015).
62. B. Vanderbeld, W. A. Snedden, Developmental and stimulus-induced expression patterns of Arabidopsis calmodulin-like genes CML37, CML38 and CML39. *Plant Mol Biol* **64**, 683-697 (2007).
63. S. Dobney, D. Chiasson, P. Lam, S. P. Smith, W. A. Snedden, The calmodulin-related calcium sensor CML42 plays a role in trichome branching. *J Biol Chem* **284**, 31647-31657 (2009).
64. H. C. Wu, D. L. Luo, F. Vignols, T. L. Jinn, Heat shock-induced biphasic Ca(2+) signature and OsCaM1-1 nuclear localization mediate downstream signalling in acquisition of thermotolerance in rice (Oryza sativa L.). *Plant Cell Environ* **35**, 1543-1557 (2012).

65. H. C. Wu, T. L. Jinn, Oscillation regulation of Ca2+ /calmodulin and heat-stress related genes in response to heat stress in rice (Oryza sativa L.). *Plant Signal Behav* **7**, 1056-1057 (2012).
66. R. Kushwaha, A. Singh, S. Chattopadhyay, Calmodulin7 plays an important role as transcriptional regulator in Arabidopsis seedling development. *Plant Cell* **20**, 1747-1759 (2008).
67. M. C. Rentel, M. R. Knight, Oxidative stress-induced calcium signaling in Arabidopsis. *Plant Physiol* **135**, 1471-1479 (2004).
68. F. Takahashi, T. Mizoguchi, R. Yoshida, K. Ichimura, K. Shinozaki, Calmodulin-dependent activation of MAP kinase for ROS homeostasis in Arabidopsis. *Mol Cell* **41**, 649-660 (2011).
69. D. Meiri, A. Breiman, Arabidopsis ROF1 (FKBP62) modulates thermotolerance by interacting with HSP90.1 and affecting the accumulation of HsfA2-regulated sHSPs. *Plant J* **59**, 387-399 (2009).
70. H. S. Jung, P. A. Crisp, G. M. Estavillo, B. Cole, F. Hong, T. C. Mockler, B. J. Pogson, J. Chory, Subset of heat-shock transcription factors required for the early response of Arabidopsis to excess light. *Proc Natl Acad Sci U S A* **110**, 14474-14479 (2013).
71. C. L. Linster, S. G. Clarke, L-Ascorbate biosynthesis in higher plants: the role of VTC2. *Trends Plant Sci* **13**, 567-573 (2008).
72. M. Mellenthin, U. Ellersiek, A. Borger, M. Baier, Expression of the Arabidopsis Sigma Factor SIG5 Is Photoreceptor and Photosynthesis Controlled. *Plants (Basel)* **3**, 359-391 (2014).
73. G. Bethke, T. Unthan, J. F. Uhrig, Y. Poschl, A. A. Gust, D. Scheel, J. Lee, Flg22 regulates the release of an ethylene response factor substrate from MAP kinase 6 in Arabidopsis thaliana via ethylene signaling. *Proceedings of the National Academy of Sciences* **106**, 8067-8072 (2009).
74. A. Mustroph, P. Juntawong, J. Bailey-Serres, Isolation of plant polysomal mRNA by differential centrifugation and ribosome immunopurification methods. *Methods Mol Biol* **553**, 109-126 (2009).
75. D. Wormuth, M. Baier, A. Kandlbinder, R. Scheibe, W. Hartung, K. J. Dietz, Regulation of gene expression by photosynthetic signals triggered through modified CO2 availability. *BMC Plant Biol* **6**, 15 (2006).
76. P. Chotewutmontri, N. Stiffler, K. P. Watkins, A. Barkan, Ribosome Profiling in Maize. *Methods Mol Biol* **1676**, 165-183 (2018).
77. Y. Liao, G. K. Smyth, W. Shi, The Subread aligner: fast, accurate and scalable read mapping by seed-and-vote. *Nucleic Acids Res* **41**, e108 (2013).
78. M. Martin, Cutadapt removes adapter sequences from high-throughput sequencing reads. *EMBnet.journal* **17**, 10 (2011).
79. B. Langmead, S. L. Salzberg, Fast gapped-read alignment with Bowtie 2. *Nat Methods* **9**, 357-359 (2012).
80. Y. Liao, G. K. Smyth, W. Shi, featureCounts: an efficient general purpose program for assigning sequence reads to genomic features. *Bioinformatics* **30**, 923-930 (2014).
81. M. D. Robinson, D. J. McCarthy, G. K. Smyth, edgeR: a Bioconductor package for differential expression analysis of digital gene expression data. *Bioinformatics* **26**, 139-140 (2010).
82. D. J. McCarthy, Y. Chen, G. K. Smyth, Differential expression analysis of multifactor RNA-Seq experiments with respect to biological variation. *Nucleic Acids Res* **40**, 4288-4297 (2012).

83. P. Juntawong, M. Hummel, J. Bazin, J. Bailey-Serres, Ribosome profiling: a tool for quantitative evaluation of dynamics in mRNA translation. *Methods Mol Biol* **1284**, 139-173 (2015).
84. R. A. Irizarry, B. M. Bolstad, F. Collin, L. M. Cope, B. Hobbs, T. P. Speed, Summaries of Affymetrix GeneChip probe level data. *Nucleic Acids Research* **31**, 15e-15 (2003).
85. Y. Benjamini, Y. Hochberg, Controlling the False Discovery Rate: A Practical and Powerful Approach to Multiple Testing. *Journal of the Royal Statistical Society* **57**, 289-300 (1995).
86. Y. Benjamini, Y. Hochberg, On the Adaptive Control of the False Discovery Rate in Multiple Testing With Independent Statistics. *Journal of Educational and Behavioral Statistics* **25**, 60-83 (2000).
87. S. Holtgrefe, J. Gohlke, J. Starmann, S. Druce, S. Klocke, B. Altmann, J. Wojtera, C. Lindermayr, R. Scheibe, Regulation of plant cytosolic glyceraldehyde 3-phosphate dehydrogenase isoforms by thiol modifications. *Physiol Plant* **133**, 211-228 (2008).
88. M. Sprenger-Haussels, B. Weisshaar, Transactivation properties of parsley proline-rich bZIP transcription factors. *The Plant Journal* **22**, 1-8 (2000).
89. A. Panda, J. Martindale, M. Gorospe, Affinity pulldown of biotinylated RNA for detection of protein-RNA complexes. *Bio-Protocol* **6**, (2016).
90. C. N. Chow, H. Q. Zheng, N. Y. Wu, C. H. Chien, H. D. Huang, T. Y. Lee, Y. F. Chiang-Hsieh, P. F. Hou, T. Y. Yang, W. C. Chang, PlantPAN 2.0: an update of plant promoter analysis navigator for reconstructing transcriptional regulatory networks in plants. *Nucleic Acids Res* **44**, D1154-1160 (2016).
91. A. Skarshewski, M. Stanton-Cook, T. Huber, S. Al Mansoori, R. Smith, S. A. Beatson, J. A. Rothnagel, uPEPperoni: an online tool for upstream open reading frame location and analysis of transcript conservation. *BMC Bioinformatics* **15**, 36 (2014).
92. D. Winter, B. Vinegar, H. Nahal, R. Ammar, G. V. Wilson, N. J. Provart, An "Electronic Fluorescent Pictograph" browser for exploring and analyzing large-scale biological data sets. *PLoS One* **2**, e718 (2007).
93. S. Lalonde, A. Sero, R. Pratelli, G. Pilot, J. Chen, M. I. Sardi, S. A. Parsa, D. Y. Kim, B. R. Acharya, E. V. Stein, H. C. Hu, F. Villiers, K. Takeda, Y. Yang, Y. S. Han, R. Schwacke, W. Chiang, N. Kato, D. Loque, S. M. Assmann, J. M. Kwak, J. I. Schroeder, S. Y. Rhee, W. B. Frommer, A membrane protein/signaling protein interaction network for Arabidopsis version AMPv2. *Front Physiol* **1**, 24 (2010).
94. P. Obrdlik, M. El-Bakkoury, T. Hamacher, C. Cappellaro, C. Vilarino, C. Fleischer, H. Ellerbrok, R. Kamuzinzi, V. Ledent, D. Blaudez, D. Sanders, J. L. Revuelta, E. Boles, B. Andre, W. B. Frommer, K+ channel interactions detected by a genetic system optimized for systematic studies of membrane protein interactions. *Proc Natl Acad Sci U S A* **101**, 12242-12247 (2004).
95. T. Seidel, D. Golldack, K. J. Dietz, Mapping of C-termini of V-ATPase subunits by in vivo-FRET measurements. *FEBS Lett* **579**, 4374-4382 (2005).
96. S. Janssen, R. Giegerich, The RNA shapes studio. *Bioinformatics* **31**, 423-425 (2015).

Figure 1: Moore et al.

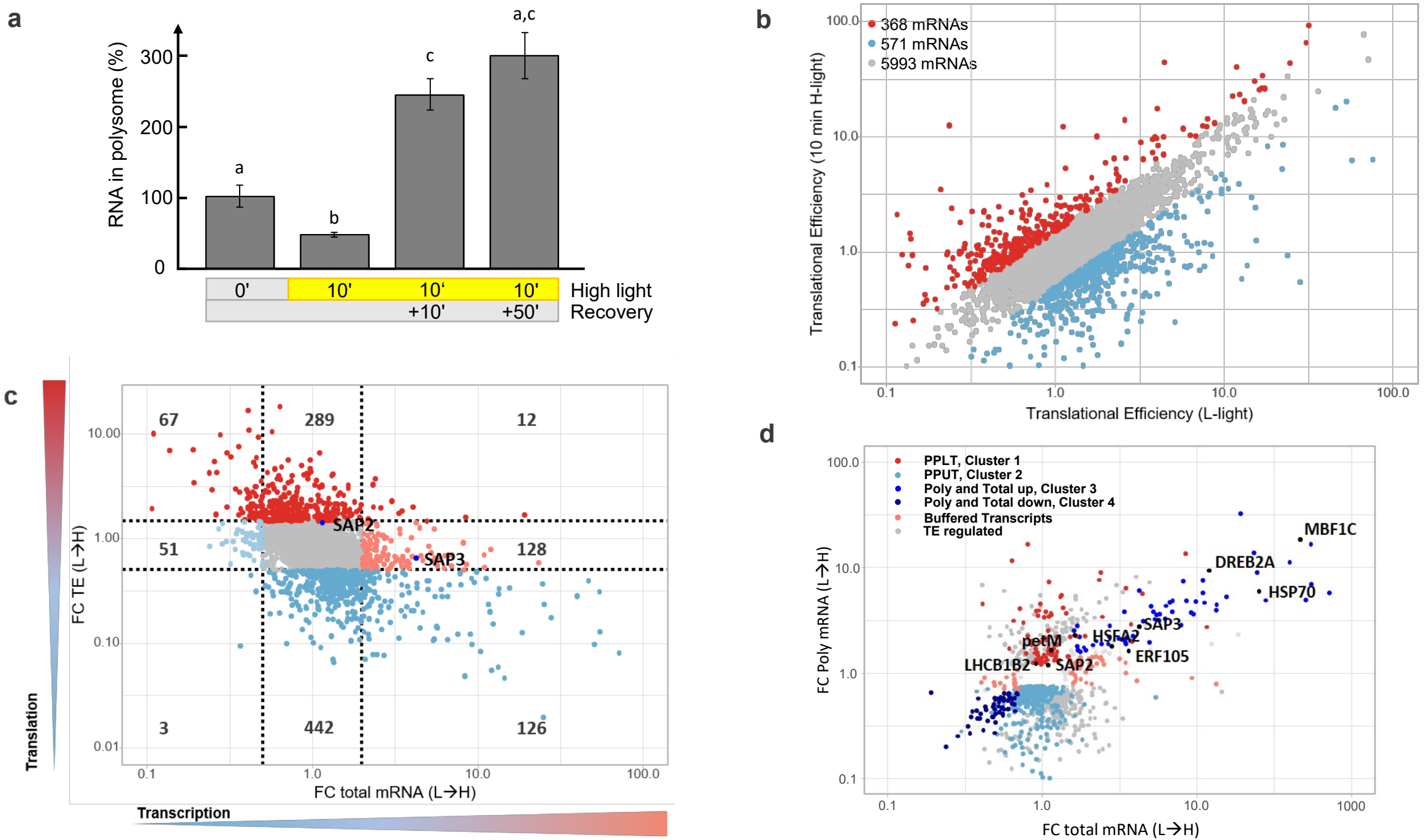

Figure 2: Moore et al.

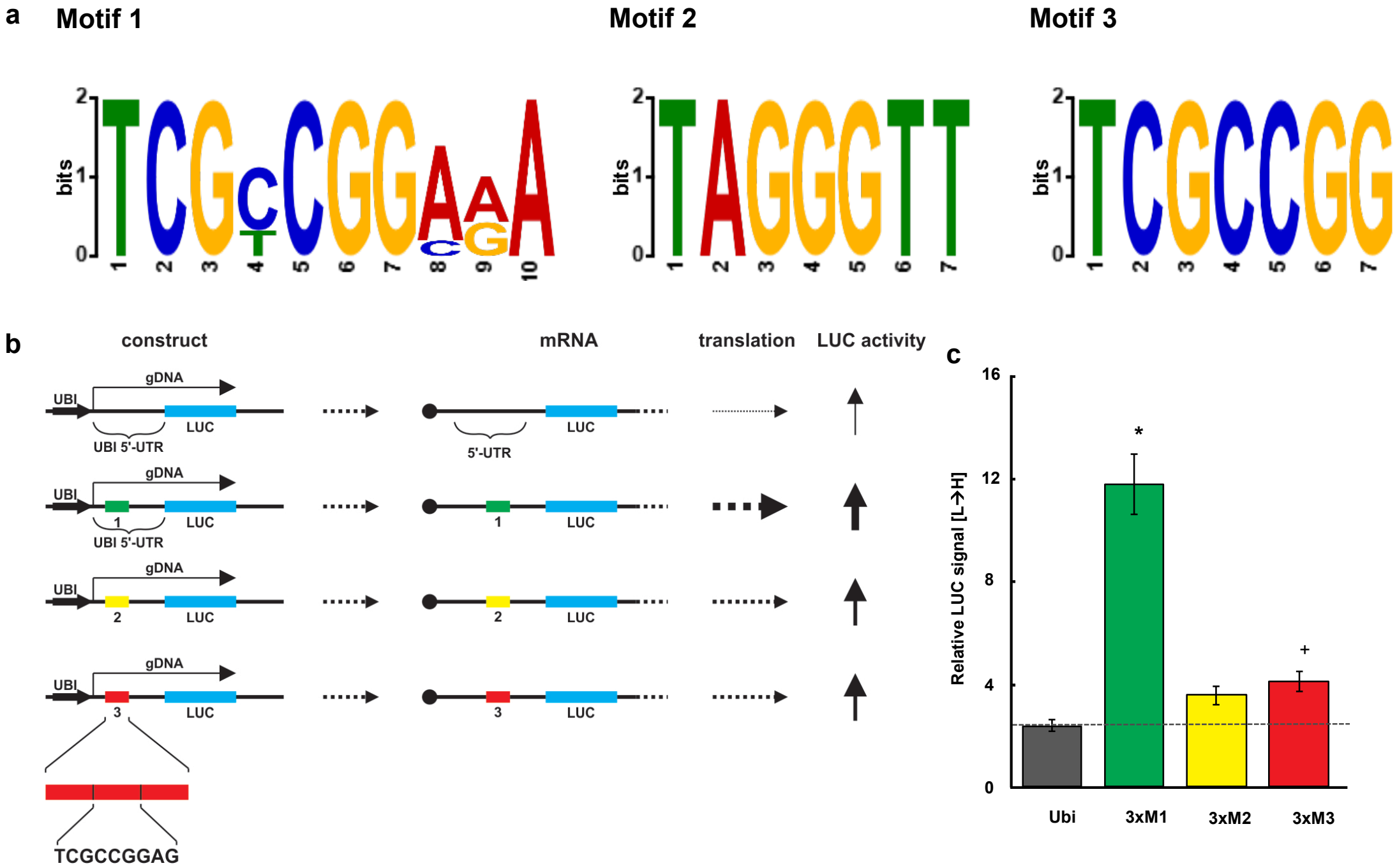

Figure 3: Moore et al.

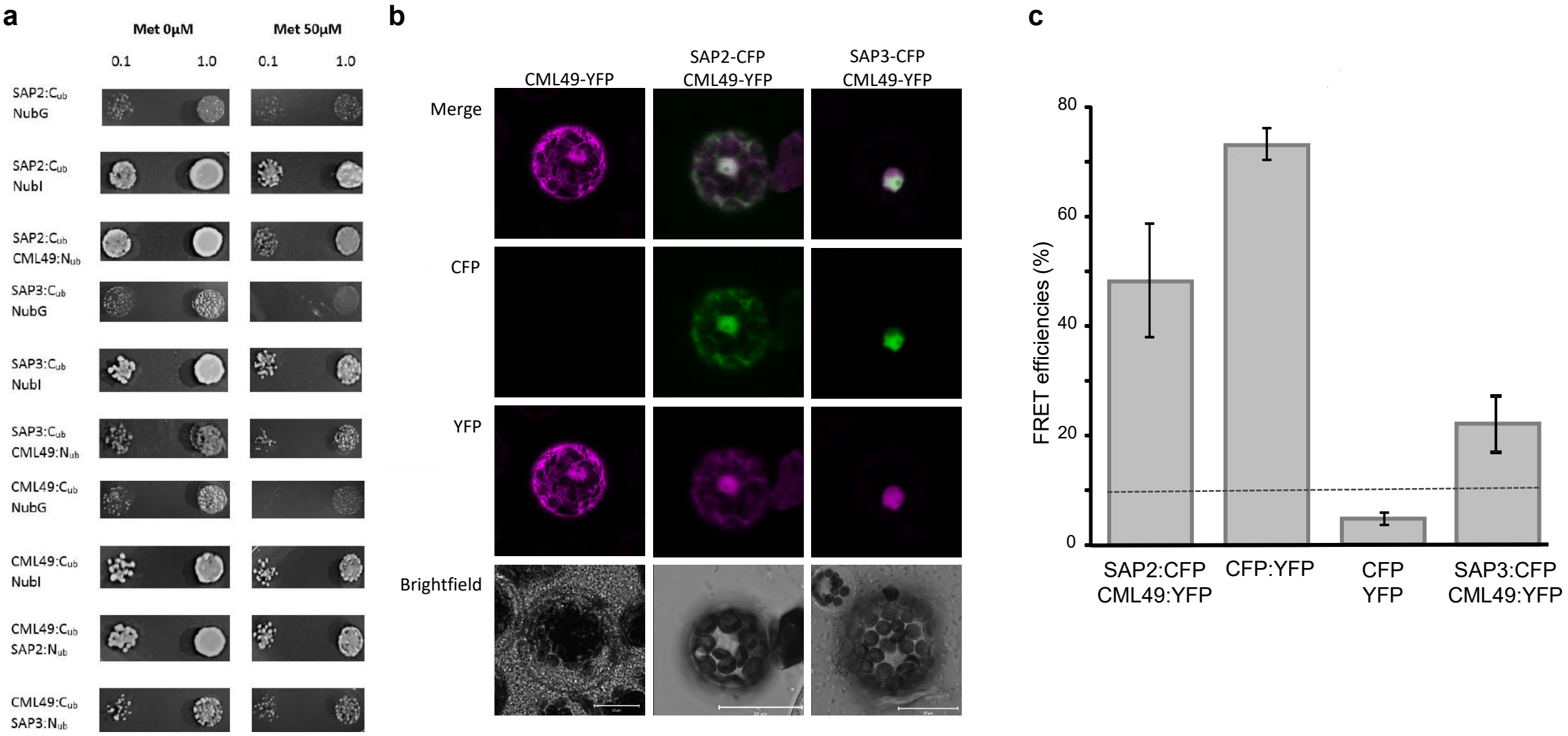

Figure 4: Moore et al.

a

Gene ID	Target	WT	*sap3 KO*	*cml49 KO*	compartment
AT4G13800	unknown				membrane, plasma membrane
AT5G52570	BETA-OHASE 2				chloroplast, chloroplast membrane
AT5G49480	CP1				cytoplasm
AT4G04020	FIB				chloroplast
AT5G58770	CPT4				nucleus
AT3G56290	unknown				mitochondrium
AT1G67360	REF				cytoplasm, vacuola
AT1G61800	GPT2				chloroplast
AT5G20150	SPX1				cytoplasm, nucleus
AT3G21890	BBX31				cytoplasm, nucleus
AT2G46830	CCA1				nucleus
AT5G52640	HSP90.1				cytoplasm
AT2G36800	DOGT1				chloroplast, membrane
AT5G48570	ROF2				cytoplasm, vacuola
AT2G24540	AFR				cytoplasm
AT3G09350	Fes1A				cytoplasm, nucleus
AT4G21990	APR3				chloroplast
AT4G12400	HOP3				cytoplasm, nucleus
AT5G50800	ATSWEET13				membrane, plasma membrane
AT2G37180	RD28				membrane, plasma
AT4G34550	PCH1-like				chromosome, cytoplasm, nucleus
AT3G17609	HYH				nucleus
AT5G64510	TIN1				chloroplast, endoplasmic reticulum
AT1G01520	ASG4				nucleus
AT1G32900	GBSS1				chloroplast
AT2G26150	HSFA2				chloroplast, cytoplasm, nucleus
AT5G12110	eEF1B				cytoplasm
AT4G26850	VTC2				cytoplasm, nucleus
AT2G33380	RD20				chloroplast membrane, endoplasmic reticulum
AT3G21150	BBX32				cytoplasm, nucleus
AT3G09450	unknown				membrane
AT2G21320	BBX18				nucleus
AT1G58520	RXW8				chloroplast
AT5G24120	SIG 5				chloroplast, mitochondrium
AT5G65380	MATE				membrane
AT3G53830	RCC1				cytoplasm, nucleus
AT3G17790	PAP17				cell surface
AT1G54050	HSP20-like				cytoplasm
AT1G62180	ATAPR2				chloroplast
AT3G21670	ATNPF6.4				membrane
AT3G12580	HSP70				membrane
AT2G46790	PRR9				nucleus
AT1G77450	NAC032				nucleus
AT2G15020	unknown				mitochondrium
AT3G47420	PS3				membrane
AT5G63130	Phox/Bem1p				nucleus
AT1G01720	ANAC2				nucleus
AT4G26150	CGA1				nucleus
AT1G74310	HSP101				chloroplast stroma, cytoplasm, cytosol, nucleus

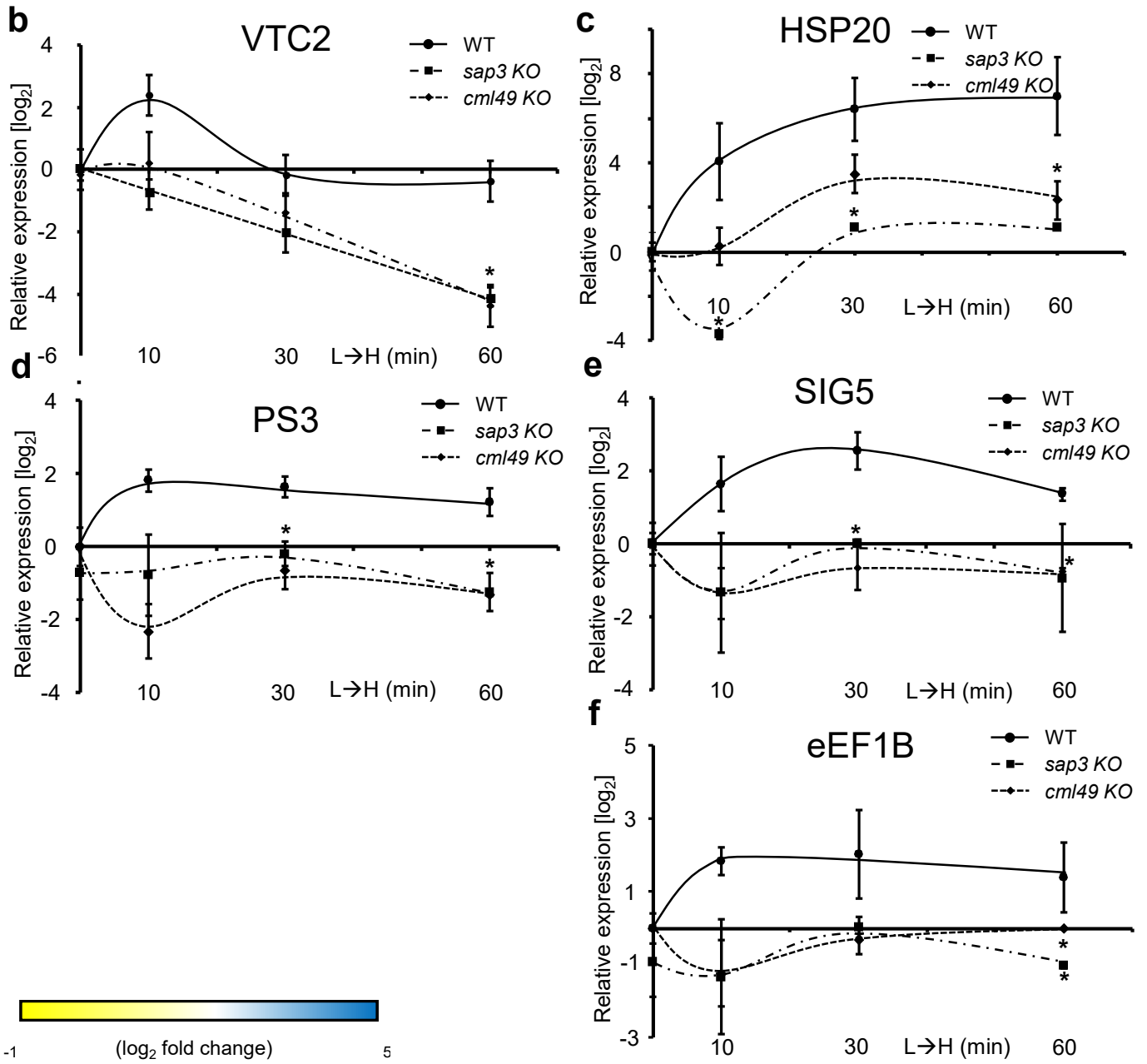
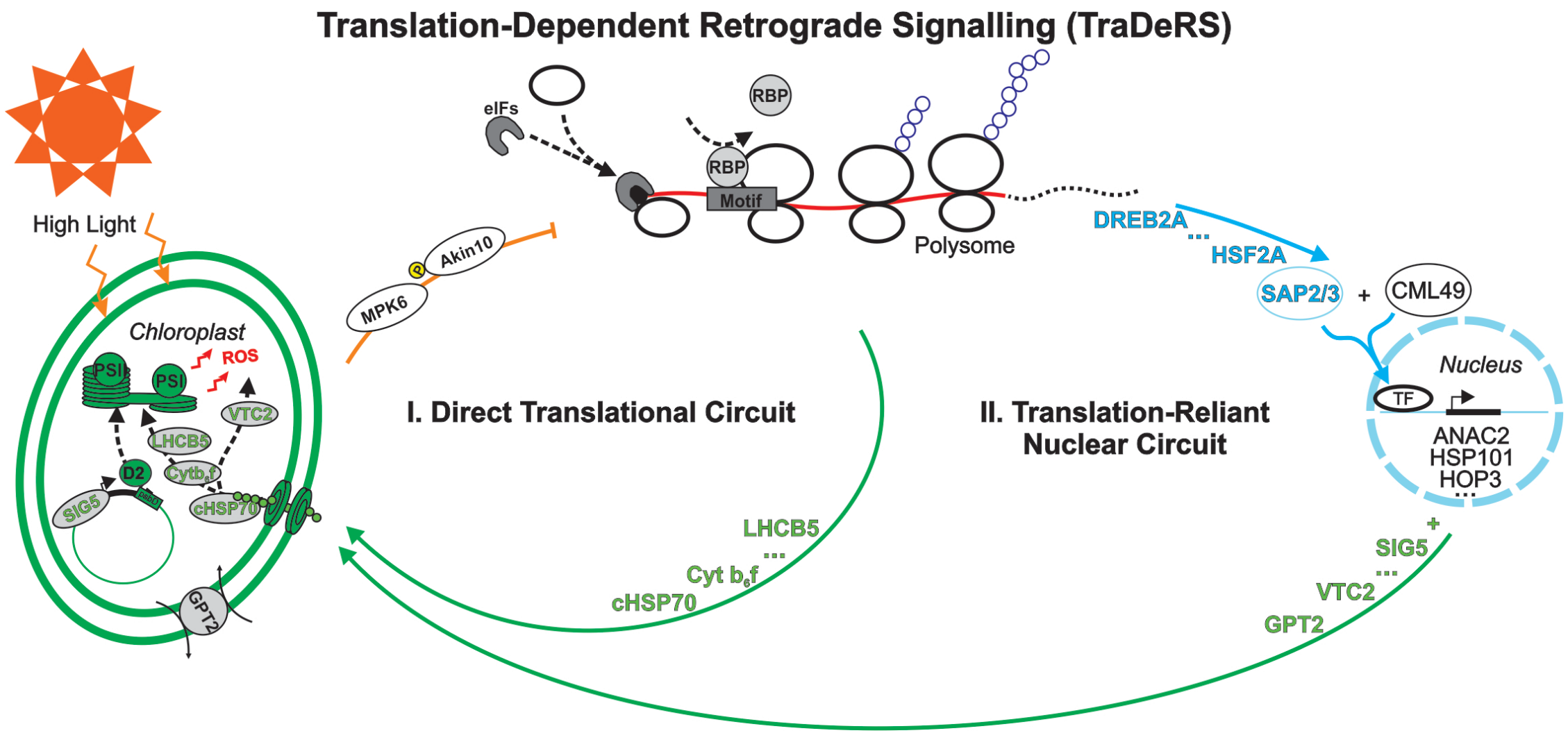
Figure 5: Moore et al.